ELSEVIER

Contents lists available at ScienceDirect

# International Journal of Fatigue

journal homepage: www.elsevier.com/locate/ijfatigue



# Fatigue failure of rivets and bolts in shear

Johan Maljaars a,b, Sjoerd Hengeveld a,b, Jorrit Rodenburg

- a TNO, Molengraaffsingel 8, Delft, 2629 JD, The Netherlands
- <sup>b</sup> Eindhoven University and Technology, Groene Loper 3, Eindhoven, 5612 AE, The Netherlands

## ARTICLE INFO

Dataset link: https://publications.tno.nl/publication/34643949/YeWIHjAo/maljaars-2025-RivetEval.xlsm

Keywords: Fatigue test database Fastener failure Riveted joints Non-prestressed bolts Double-covered joints Bridges

## ABSTRACT

Double-covered shear joints with hot rivets or with snug tight bolts subjected to cyclic load may fail in the ply or in the fastener. Tests with the latter failure mode are sparse and scattered. This paper combines these data and attempts to provide a unified theory on the fatigue driving force for this failure mode. Using the finite element method, we demonstrate that the nominal shear stress in the fastener is not a good indicator of its fatigue performance, because it ignores frictional force transfer and assumes an equal load share between fasteners. We provide an analytical model for the actual shear stress range. We derive S–N curves for this shear stress range, either using straightforward regression of test data or using Bayesian inference of the decisive failure type (ply or fastener). Finally, we derive the geometries and loads for which fastener failure is decisive over ply failure.

#### 1. Introduction

Almost all bridges constructed before 1950, and many bridges between 1950 and 1970, contain hot-riveted joints. Many of these bridges are still in service to date. The current numbers of freight transports were not foreseen in the design of these bridges, which makes the fatigue performance of riveted shear joints a subject of ongoing study [1–3]. Contraction during cooling of the rivets after driving causes a certain clamping stress in the rivet [4], but the clamping stress is often too small for full force transfer through friction. Hence, part of the force is transferred through bearing.

Inspections of fatigue-loaded bolted joints, in which the bolts are intended to be prestressed, occasionally reveal loose bolts. In addition, snug-tight (non-prestressed) bolts are applied in light structures such as racks. These structures can also be subject to fatigue loads [5].

The load transfer and fatigue performance of shear joints with partially or non-prestressed fasteners (bearing-type joints) differs from that of fully prestressed fasteners (slip-resistant joints) [6,7]. Bearing-type double-covered shear joints subjected to cyclic load, Fig. 1, can show three types of failure, namely (Fig. 2):

- Failure in the net section of the ply loaded in cyclic tension (or tension-compression) — Failure Type 1 (FT1);
- Failure in the net section of the strap loaded in cyclic tension (or tension–compression) — FT2;
- 3. Failure of the fastener in cyclic shear FT3.

We have developed an analytical model and derived an S–N curve for FT1 in [8]. This model estimates the stress range in the ply at the edge of the hole, which we call the hoop stress range  $\Delta\sigma_h$ . The fatigue resistance correlates much better with the hoop stress range than with the net section stress range used by others [9–12]. FT2 rarely occurs for joint strap thickness equal to or larger than the ply thickness [8]  $(2t_s \geq 2t_p)$ , see Fig. 1 for the symbols) and we therefore do not consider it.

FT3 remains to be studied. For rivets, DiBaptista et al. [10] conclude that most fatigue failures occur in the connected plates and not in the rivet. However, [13–15] occasionally report FT3 in their tests. Wilson [16] reports test series on relatively thick plates aimed at FT3. Based on these and similar tests, [11,17] provide S–N curves using the following nominal rivet shear stress range as the fatigue driving force:

$$\Delta \tau_n = \frac{\Delta F}{n_s n_{row} n_{pr} \pi r_r^2} \tag{1}$$

where F is the load applied to the joint,  $n_s$  is the number of shear planes (equal to two in double-covered shear joints),  $n_{row}$  is the number of rivet rows perpendicular to the direction of applied load (Fig. 1),  $n_{pr}$  is the number of rivets per row in line with the applied force (Fig. 1), and  $r_r$ , depending on the literature source, is usually the nominal rivet shaft radius  $r_r$ , and sometimes the hole radius  $r_r$ .

With respect to bolts, the thread can extend beyond the shear plane, or it can stop before the shear plane, see Fig. 3(a) and (b), respectively. In the former case, FT3 occurs in the threaded section, resulting in low

<sup>\*</sup> Corresponding author at: Eindhoven University and Technology, Groene Loper 3, Eindhoven, 5612 AE, The Netherlands. E-mail address: johan.maljaars@tno.nl (J. Maljaars).

Nomenclature	
Symbols	
$\beta_1$	Bearing ratio of first fastener row
$\chi_{k, au}, \chi_{k,\sigma}$	Relative distance of test $k$ to the centroid of
$\Delta X$	the data (for fastener failure, for ply failure) Range of cycle <i>X</i>
$\hat{X}$	Estimate or expectation of <i>X</i>
K	Normalization parameter
	Friction coefficient
$\mu$	Poisson ratio
v _	Stress in the ply at the fastener hole ('hoop
$\sigma_h$	stress')
$\sigma_{cl},\sigma_{cl,0}$	Rivet clamping stress (before load application)
$\sigma_{cx}$	Contact stress in direction of applied load
$\sigma_{net}$	Net section stress
$ au,  au_C  au_{FE},  au_h,  au_n$	Fastener shear stress (characteristic value, according to the FE method, the analytical model, nominal)
_ ζ	Curvature parameter for unloading curve
a	Hutchinson's factor
$A_c$	Contact area
$C_{\tau}, C_{\sigma}$	Ordinate intercept of the Basquin equation (for fastener failure, for ply failure)
E	Young's modulus
e	End distance
F	Applied load
$f_1$	Force fraction transferred at first fastener row
$f_{P}(Y)$	Prior of Y
$F_s$	Shear force per shear plane
$f_X(X)$	Probability density of X
$F_{slip}$	Slip force per fastener
G	Shear modulus
h	Semi grip
K	Hoop stress correction factor
$k_p, k_r, k_s$	Spring stiffness (of the ply, fastener, strap)
$m_{\tau}, m_{\sigma}, m_{\alpha}$	Inverse slope of the Basquin equation (for
	fastener failure, for ply failure, or with exceedance probability $\alpha$ )
$N_{ au}, N_{\sigma}$	Number of cycles to failure (for fastener
	failure, for ply failure)
$n_{\tau}, n_{\sigma}, n_{r}, n_{tot}$	Number of tests (with shear failure, with ply
	failure, run-outs, total)
$n_{pr}$	Number of fasteners per row
$n_{row}$	Number of fastener rows
I	

fatigue resistance [7]. Therefore, most modern standards and guidelines [18–20] require non-threaded shaft in the shear planes. Our study considers this condition. The nominal shear stress is as in Eq. (1), where  $r_r$  is the radius of the bolt shaft.

Opposed to Eq. (1), the force transfer is usually not equally distributed over the fastener rows [16]. Depending on the geometry, the first fastener row transfers a larger fraction of force than the adjacent rows. In addition, a certain fraction of force is transferred through friction between the plates, depending on the fastener prestress  $\sigma_{cl,0}$  and the friction coefficient  $\mu$ . As a result, a higher fatigue resistance is observed for a higher prestress [21]. Eq. (1) therefore represents a

$n_{s}$	Number of shear planes
p	Pitch
$P_i$	Probability of fastener failure of test <i>i</i>
R	Load ratio
r	Hole radius
$R_h$	Ratio of the hoop stress
$r_o$	Cone outer radius
$r_r$	Hole or fastener radius
$R_{sq}$	Coefficient of determination
$s_{\tau}, s_{\sigma}$	Standard deviation of the Basquin equation (for fastener failure, for ply failure)
$T(\alpha, \text{DOF})$	Cumulative probability of the student $T$ distribution with exceedance probability $\alpha$ and DOF degree of freedom
$t_p$	Semi ply thickness
$t_s$	Thickness of one strap or lap plate
$t_{(\alpha, \text{DOF})}$	Inverse of the student $T$ distribution with exceedance probability $\alpha$ and DOF degree of freedom
$u_{j,p}, u_{j,s}$	Deformation of node $j$ (of the ply, strap)
w	Semi gauge for center rivets, or average between edge distance and semi gauge for rivets at plate edge
$x_i, x_C$	10-base logarithm of the stress range [MPa] (of test <i>i</i> , characteristic value)
$y_i, y_{i,\alpha}$	10-base logarithm of the number of cycles to failure of test $i$ (with exceedance probability $\alpha$ )
Superscripts	
*	Using a predefined ('fixed') slope parameter
max	At maximum load of the cycle
min	At minimum load of the cycle

rough approximation of the actual (average) shear stress per fastener shear plane.

The purpose of this paper is two-fold. First, we derive S-N curves for FT3 using the actual (average) shear force transferred per fastener. Second, we derive the joint dimensions at which FT3 dominates over FT1. This study is limited to double-covered shear joints. Fasteners may skew in single lap joints, causing a different load on the fastener that is not covered in this study. Section 2 describes the methods, including the finite element (FE) method to evaluate the shear force transferred per shear plane, the derivation of the analytical model to estimate this shear force, the regression analysis of fatigue test data, and the equations to distinguish between FT1 and FT3. The description of the fatigue tests, collected from the literature, forms the subject of Section 3. Section 4 gives the results, including lessons learned from the FE method, a comparison between the shear stress according to the analytical model and the FE method, the derivation of the S-N curves for FT3 and the joint geometries for which FT3 is decisive over FT1. Section 5 provides the conclusions.

# 2. Models and methods

## 2.1. Finite element models

The FE models that we employ to estimate the shear force are the same models as elaborated in [8] and they are inspired on work of others [22–30]. All models, analyzed with the commercial FE software Abaqus version 2020 HF2, represent double-covered shear joints ( $n_s$  =

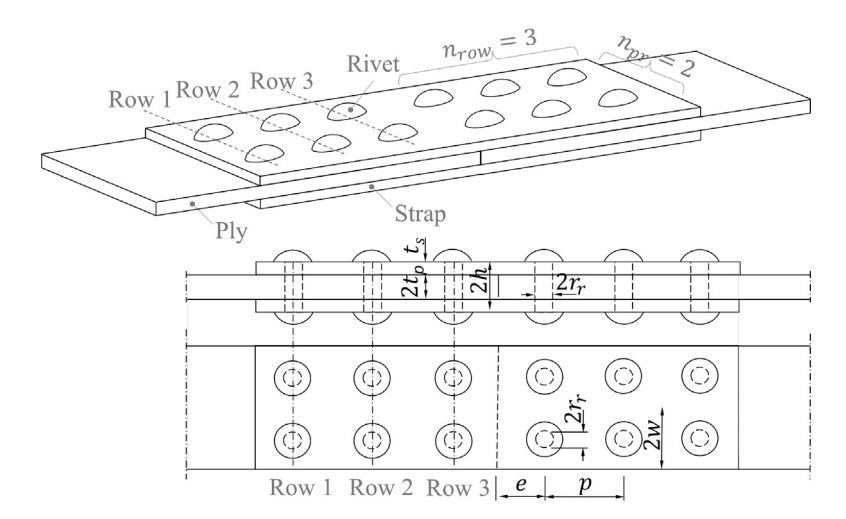
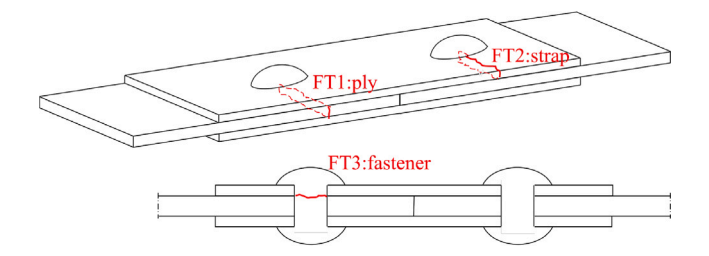


Fig. 1. Lay-out of a double-covered shear joint with 3 rows per side  $(n_{row} = 3)$  and 2 fasteners per row  $(n_{pr} = 2)$ .



**Fig. 2.** Three failure types of bearing-type double-covered shear joints: net section of the ply in tension (FT1), net section of the strap in tension (FT2), or fastener in shear (FT3).

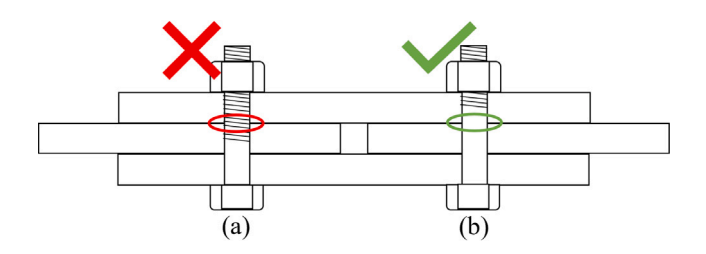


Fig. 3. Extent of thread in a bolt: (a) Beyond the shear plane, not considered in this study; (b) Before the shear plane, subject of this study.

- 2). The rivets are modeled as hole-filling after driving  $(r_r=r)$ , following experimental observations in [13,16,31]. The models represent 1/8 of the complete geometry and consist of hexahedral elements of type C3D20R (quadratic shape function and reduced integration scheme) for plates and fasteners, Fig. 4(a). These components have linear elastic material with Young's modulus E=210 GPa and Poisson ratio v=0.3. Contact interactions with a Lagrange penalty model in the normal direction and a Coulomb friction model in the tangential direction represent the interfaces between the components. The friction coefficient varies per simulation, see Section 3.3. The interactions cause the model to behave non-linear despite the linear elastic material of the steel components. The simulations consist of three load stages, each consisting of multiple increments:
  - 1. The clamping stress of the fastener is applied by assigning a temperature change to the fastener shaft, which has a predefined thermal expansion coefficient. The temperature change is determined by trial so that the desired clamping stress is obtained. The applied clamping stress varies per simulation, see Section 3.3.

- 2. The maximum external load is applied to the ply.
- 3. The minimum external load is applied to the ply.

We evaluate the average shear stress range in the shear plane:

$$\Delta \tau_{FE} = \frac{\Delta F_s}{\pi r^2} \tag{2}$$

$$F_s = \int_A \sigma_{cx} dA \tag{3}$$

where  $F_s$  is the shear force per shear plane, obtained from the integral of the contact stress between fastener and ply, see Fig. 4(b),  $A_c$  is the contact area and  $\sigma_{cx}$  is the contact stress in the direction of the applied load (x-direction). Simulations with Stages 2 and 3 repeated multiple times show that the stress distribution does not change after the first unloading cycle (second half cycle), as explained in Fig. 4(c). The shear force range  $\Delta F_s$  is therefore equal to the arithmetical difference between the shear forces in analysis Stages 2 and 3.

## 2.2. Analytical model for fastener shear force

Using mechanical principles, the average shear stress range in the fastener can be estimated through a number of closed-form equations, hereafter called analytical model. This model accounts for the effects of frictional force transfer (for rivets and for semi-prestressed bolts) and non-uniform force transfer between the different rows of fasteners. Fig. 5(a) explains two terms used in the model: The fraction  $f_1$  denotes the force share transferred by the first (outer) row of fasteners (see Fig. 1), which is the decisive row [16]. The slip force  $F_{slip}$  is the maximum force transferred through friction per fastener. The part of the force exceeding  $F_{slip}$  is transferred through bearing and this part causes shear stress in the fastener.

The shear stress range used here is the average shear stress per shear plane at maximum applied load minus that at minimum applied load:

$$\Delta \tau_h = \frac{F_s^{max} - F_s^{min}}{\pi r_r^2} \tag{4}$$

where subscripts  $^{max}$  and  $^{min}$  refer to maximum and minimum applied load, respectively. We use the hole radius  $r_r = r$  for rivets in Eq. (4) because driven rivets after cooling are almost hole-filling. Upon first loading (Stage 2), a fastener shear force builds up if the applied load exceeds the slip force, see the red dashed curve in Fig. 5(c). The shear force in this stage follows from:

$$F_s^{max} = F^{max} \frac{f_1 \beta_1^{max}}{n_s n_{pr}} \tag{5}$$

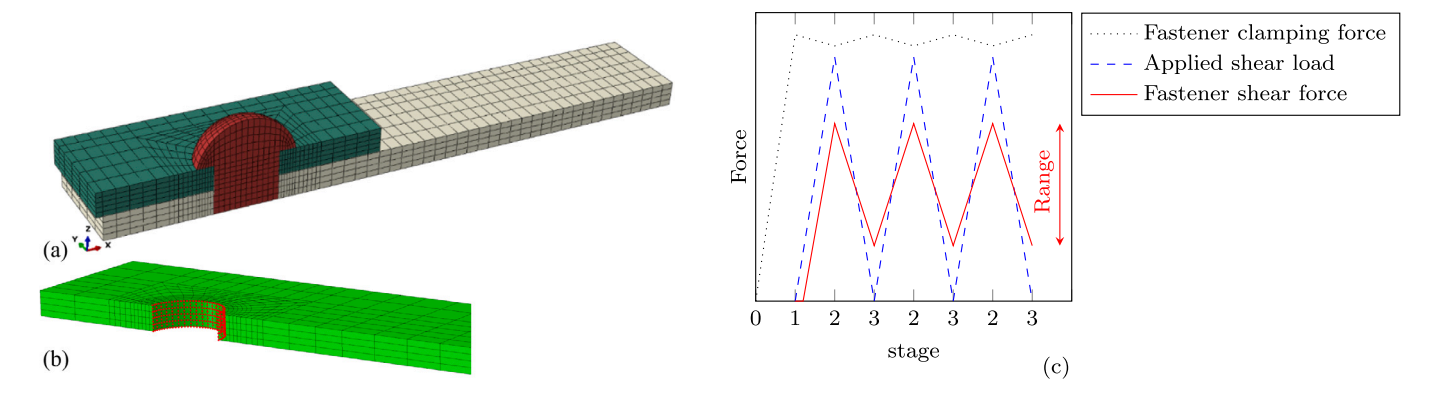


Fig. 4. Finite element method employed to evaluate the rivet shear stress: (a) Lay-out of the model; (b) Contact area used to determine the shear force; (c) Schematic of the fastener force versus the applied load.

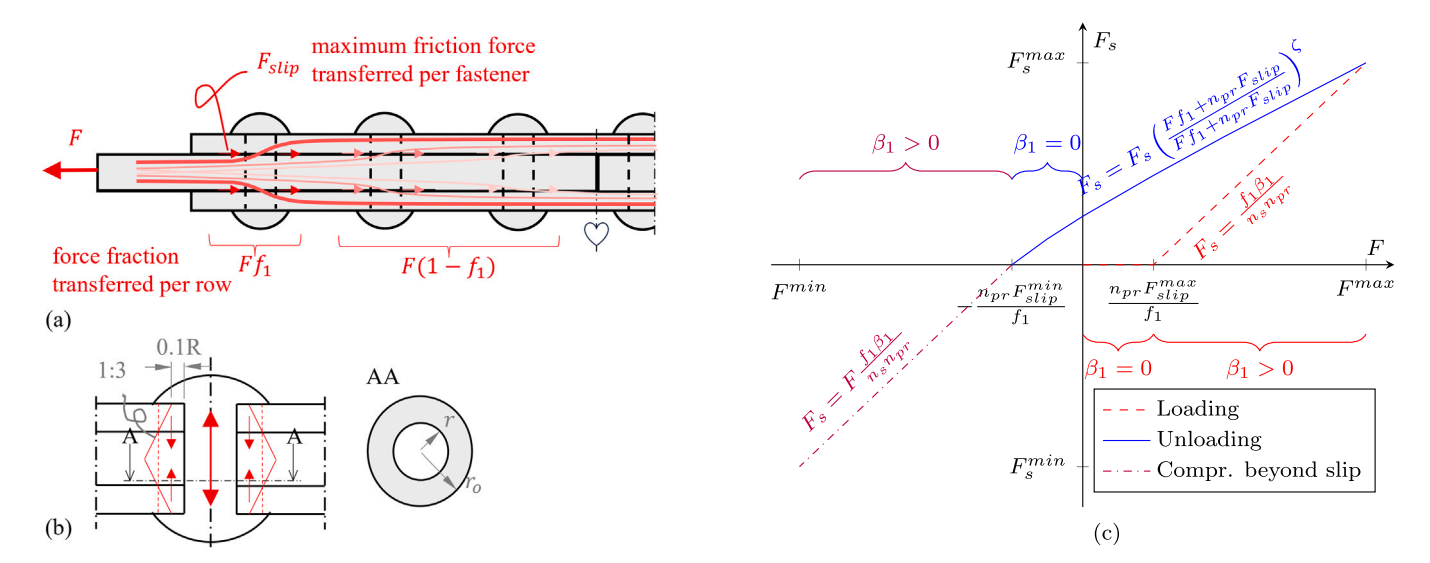


Fig. 5. Explanation of the analytical model: (a) Terminology  $f_1$  and  $F_{slip}$ ; (b) Compression cone around fastener; (c) Shear force per fastener  $F_s$  as a function of the applied load

where  $\beta_1$  is the ratio between the bearing force and the total force per fastener in the first row. It ranges between 0 and 1 for loads fully transferred by friction and by bearing, respectively. For a given applied maximum load in between these two extremes [8]:

$$\beta_1^{max} = \max\left(0, \frac{|f_1 F^{max}| - n_{pr} F_{slip}^{max}}{|f_1 F^{max}|}\right)$$
 (6)

The slip force per fastener is approximated by:

$$F_{slip}^{max} = n_s \mu \sigma_{cl}^{max} \pi r_r^2 \tag{7}$$

where  $\mu$  is the friction coefficient between the plates and  $\sigma_{cl}$  is the fastener clamping stress. The latter depends on the applied load because of lateral contraction of the plates. It is estimated with [8]:

$$\sigma_{cl}^{max} = \max\left(0, \sigma_{cl,0} - \nu \sigma_{net}^{max} \frac{t_p}{h} \frac{r_o^2 - r^2}{r_o^2}\right)$$
 (8)

where  $t_p$  is the semi ply thickness, h is the semi grip (see Fig. 1),  $r_o$  is the radius of the cone that transfers the compression stress in the plates,  $\sigma_{cl,0}$  is the initial clamping stress of the fastener (without applied load on the joint) and  $\sigma_{net}$  is the net section stress in the ply:

$$\sigma_{net}^{max} = \frac{F^{max}}{n_{pr}(2w - 2r)2t_p} \tag{9}$$

where w is the semi gauge distance for center fasteners, or the average between semi gauge distance and edge distance for the fasteners closest

to the plate edge (see Fig. 1). The fastener cone radius is approximated with, see Fig. 5(b):

$$r_o = 1.1r + h/3 \tag{10}$$

where the factor of 3 is a load spread factor [32] and 1.1r is an estimate of the load carrying radius of the rivet head [8].

Force fraction  $f_1$  in Eqs. (5)–(6) can be estimated with a linear spring model [8]:

$$f_1 = 2k_r(u_{1,p} - u_{1,s})n_{pr}/F^{max}$$
(11)

where  $k_r$  is the fastener stiffness and  $u_{1,p}-u_{1,s}$  is the relative displacement between the ply and strap at the first row. For an example joint with  $n_{row}=2$  and  $n_{pr}=1$ , these relative displacements follow from solving the following matrix, Fig. 6:

$$\begin{bmatrix} F^{max}/2 \\ 0 \\ 0 \\ -F^{max}/2 \end{bmatrix} = \begin{bmatrix} k_p + k_r & -k_p & -k_r & 0 \\ -k_p & k_p + k_r & 0 & -k_r \\ -k_r & 0 & k_s + k_r & -k_s \\ 0 & -k_r & -k_s & k_s + k_r \end{bmatrix} \begin{bmatrix} u_{1,p} \\ u_{2,p} \\ u_{1,s} \\ 0 \end{bmatrix}$$
(12)

with the following compliances of the ply, the strap, and the fas-

$$\frac{1}{k_p} = \frac{p - 2r}{2wt_p E} + \frac{2r}{2(w - r)t_p E} \tag{13}$$

$$\frac{1}{k_s} = \frac{p - 2r}{2wt_s E} + \frac{2r}{2(w - r)t_s E} \tag{14}$$

Fig. 6. Explanation of the spring model in Eq. (12): (a) Joint considered; (b) Spring components.

$$\frac{1}{k_r} = \frac{9t_s^3 + 48t_s^2t_p + 64t_st_p^2 + 16t_p^3}{96E\pi r^4} + \frac{4t_p + 3t_s}{8aG\pi r^2} + \frac{1}{t_pE} + \frac{1}{t_sE} + \frac{1}{2t_pE}$$
(15)

$$a = \frac{6(\nu+1)^2}{4\nu^2 + 12\nu + 7}$$

where G = E/(2[1+v]) is the shear modulus, p is the pitch, and  $t_s$  is the full thickness of one strap. Similar matrices can be derived for different joint configurations.

Upon unloading, the shear force reduces to zero if the applied load just causes slip in compression. The built-up slip force in tension gradually releases during unloading, and it again builds up gradually if loaded in compression. Hence, the shear force reduces approximately linearly between its maximum and zero for a decreasing applied load between the maximum applied load and the slip force in compression; see the blue solid curve in Fig. 5(c). For an applied compressive load that is lower than the slip force in compression, a similar equation as Eq. (5) applies; see the purple dash-dotted curve in Fig. 5(c). The shear force in the unloading stage hence follows from:

$$F_{s}^{min} = \begin{cases} F_{s}^{max} \left( \frac{F^{min} f_{1} + n_{pr} F_{slip}^{min}}{F^{max} f_{1} + n_{pr} F_{slip}^{min}} \right)^{\zeta} & \text{if } F^{min} \geq -n_{pr} F_{slip}^{min} / f_{1} \\ F^{min} \frac{f_{1} \theta_{1}^{min}}{n_{s} n_{pr}} & \text{if } F^{min} < -n_{pr} F_{slip}^{min} / f_{1} \end{cases}$$

$$(16)$$

where  $\zeta$  is a calibration parameter introduced because the FE simulations with  $\mu>0$  show a slight non-linear unloading path. Based on the FE simulations:

$$\zeta \approx 1 - \mu/3 \tag{17}$$

Quantities  $\rho_1^{min}$  and  $F_{slip}^{min}$  follow from similar equations as for the loading stage, Eqs. (6)–(9).

For convenience, we implemented all equations in a MS Excel sheet, which readers can download from Appendix A of the online version of this paper.

## 2.3. Evaluation method of fatigue test data

We use the well-known Basquin equation as the S-N curve:

$$\log_{10}(N_{\tau}) = C_{\tau} + m_{\tau} \log_{10}\left(\frac{\Delta \tau}{\text{MPa}}\right)$$
 (18)

where  $N_{\tau}$  is the number of cycles at which the fastener failed and parameters  $C_{\tau}$  and  $m_{\tau}$  follow from the regression of the test data. Two frequentist methods are often applied for the regression, namely, least squares and maximum likelihood. Although maximum likelihood offers some advantages [33–35], the least squares method is more often used for deriving S–N curves in standards [36,37]. We therefore used the latter method, of which the regression procedure is described extensively in [38,39]. Using notations  $y = \log_{10}(N_{\tau})$ ,  $x = \log_{10}(\frac{\Delta \tau}{\text{MPa}})$ , and the hat symbol as estimator, the life estimator of a future test k in case of a limited number of available fatigue test data is:

$$\hat{y}_k = \hat{C}_\tau + \hat{m}_\tau x_k \tag{19}$$

$$\hat{m}_{\tau} = \frac{n_{\tau} \sum_{i} (x_{i} y_{i}) - \sum_{i} (x_{i}) \sum_{i} (y_{i})}{n_{\tau} \sum_{i} (x_{i})^{2} - \left[\sum_{i} (x_{i})\right]^{2}}$$
(20)

$$\hat{C}_{\tau} = \frac{\sum_{i} (y_i)}{n_{\tau}} - \frac{\hat{m}_{\tau} \sum_{i} (x_i)}{n_{\tau}}$$
(21)

where  $i \in (1..n_{\tau})$  is the *i*th conducted test that failed in FT3 (fastener failing in shear). This procedure ignores tests terminated before failure,

so-called run-outs. Assuming a normal distribution for the difference between the actual life and the predictor with the Basquin equation, the 5% and 95% prediction bounds of the life of a future test k follow from:

$$y_{k,0.05}; y_{k,0.95} = \hat{y}_k \pm t_{(0.95,n_\tau - 2)} s_\tau \sqrt{1 + \frac{1}{n_\tau} + \chi_{k,\tau}}$$
 (22)

where  $t_{(0.95,n_\tau-2)}$  is the inverse of the student's t distribution for  $n_\tau-2$  degrees of freedom evaluated at a fraction of 95%,  $s_\tau$  is the standard deviation of the number of cycles to failure:

$$s_{\tau} = \sqrt{\frac{\sum_{i} (y_{i} - \hat{y}_{i})^{2}}{n_{\tau} - 2}} \tag{23}$$

and  $\chi_{k,\tau}$  is the relative distance between the shear stress range of future test k and the centroid of the test data:

$$\chi_{k,\tau} = \frac{\left[ x_k - \sum_i (x_i) / n_\tau \right]^2}{\sum_i \left[ x_i - \sum_i (x_i) / n_\tau \right]^2}$$
(24)

Contrary to the prediction bounds for the future test k, we use confidence bounds to show the scatter of other variables. The 5% and the 95% confidence bounds of the reciprocal slope parameter follow from:

$$\begin{split} m_{0.05}; m_{0.95} &= \hat{m_\tau} \pm \frac{t_{(0.95, n_\tau - 2)} s_\tau}{\sqrt{\sum_i \left[ x_i - \sum_i (x_i) / n_\tau \right]^2}} \\ \text{S-N curves for design purposes usually have a predefined slope} \end{split}$$

S–N curves for design purposes usually have a predefined slope parameter, with a value of e.g.  $m^* = -3$  or -5. The corresponding characteristic reference fatigue resistance  $\Delta \tau_C$ , defined as the 95% prediction bound at  $N = 2 \cdot 10^6$  cycles, follows from the procedure in [37]. It uses a Bayesian estimate of the variables under limited available data [40]:

$$\Delta \tau_C = 10^{x_C} \text{ MPa} \tag{26}$$

$$x_C = \frac{\log_{10}(2 \cdot 10^6) - \hat{C}_{\tau}^* + s_{\tau}^* t_{(0.95, n_{\tau} - 1)} \sqrt{1 + 1/n_{\tau}}}{m_{\tau}^*}$$
 (27)

$$\hat{C}_{\tau}^* = \frac{\sum_{i} (y_i)}{n_{\tau}} - \frac{m_{\tau}^* \sum_{i} (x_i)}{n_{\tau}}$$
 (28)

$$s_{\tau}^* = \sqrt{\frac{\sum_i (y_i - \hat{C}_{\tau}^* - m_{\tau}^* x_i)^2}{n_{\tau} - 1}}$$
 (29)

#### 2.4. Evaluation method for decisive failure type

The evaluation of the decisive failure type of a given joint (either FT1 — ply failure or FT3 — fastener failure) requires the S–N curves of both failure types. Ref. [8] contains a model to estimate the maximum stress range at the hole edge in the ply,  $\sigma_h$ . The MS Excel sheet that can be downloaded from Appendix A has the corresponding equations implemented. The associated S–N curve for FT1 is:

$$\log_{10}(N_{\sigma}) = C_{\sigma} + m_{\sigma} \log_{10} \left( \frac{\Delta \sigma_h / K}{\text{MPa}} \right)$$
 (30)

$$K = 3.16 \frac{1 - R_h}{1 - 0.9 R_h} \tag{31}$$

where  $N_{\sigma}$  is the number of cycles to failure in FT1 and  $R_{h}$  is the stress ratio of the hoop stress at the hole edge. The value of 3.16 in Eq. (31)

is a scale factor, taken equal to the mean of the stress concentration factor of all tests in [8].

Using the S–N curves of the two failure types, we can estimate the probability that FT3 governs over FT1 of a joint with a given lay-out. A closed-form solution of this probability exists if the number of available tests with FT1 equals that of FT3, so that the Degrees Of Freedom (DOF) are equal for both failure types:

$$P_k \left( N_{\tau} < N_{\sigma} \right) = T(-z_k, \text{DOF}) \tag{32}$$

where T is the cumulative distribution function of the Student T distribution and

$$z_k = \frac{\hat{C}_{\tau} + \hat{m}_{\tau} \log_{10} \left(\frac{\Delta \tau}{M \text{Pa}}\right) - \hat{C}_{\sigma} - \hat{m}_{\sigma} \log_{10} \left(\frac{\Delta \sigma/K}{M \text{Pa}}\right)}{\sqrt{s_{\tau}^2 (1 + \chi_{k,\tau}) + s_{\sigma}^2 (1 + \chi_{k,\sigma})}}$$
(33)

where  $s_{\sigma}$  and  $\chi_{\sigma}$  are similar as their shear stress counterparts of Eqs. (23)–(24). For the general case that the number of tests of the two failure types are not equal, a conservative estimate of the confidence interval results by taking DOF in Eq. (32) equal to the minimum of  $n_{\tau}-2$  and  $n_{\sigma}-2$ .

Using Eq. (32) as a basis, the failure types of the fatigue tests conducted allow us to estimate the Basquin curve of one failure type, given the Basquin curve of the other failure type. This is a different strategy from the standard regression mentioned above to derive an S-N curve, although it partially relies on the same test data. Based on the many test data collected in [8], the parameters of the Basquin curve of FT1 are relatively certain. Using a predefined slope parameter  $m_{\tau}^*$ , we employ Bayesian inference to estimate the Basquin curve of FT3:

$$f_{C_{\tau}^*}(C_{\tau}^*|\text{failure types of tests}) = \frac{L(\text{failure types of tests}|C_{\tau}^*)f_P(C_{\tau}^*)}{f_{ft}(\text{failure types of tests})}$$

where  $f_{C_\tau}(C_\tau|\text{failure types of tests})$  is the posterior distribution of  $C_\tau$  given the failure type of all tests,  $L(\text{failure types of tests}|C_\tau)$  is the likelihood of the failure type of the tests given  $C_\tau$ ,  $f_P(C_\tau)$  is the prior or initial belief of  $C_\tau$ , and  $f_{ft}(\text{failure types of tests})$  is the probability of observing the failure types of the tests. Here, we make use of an uninformed prior for  $C_\tau$ , i.e.,  $f_P$  has a uniform distribution without bounds (note that we use a fully informative prior for the slope parameter). Further, we use the natural logarithm of the likelihood to prevent inaccuracy in case of low probabilities. The posterior can then be determined with:

$$f_{C_{\tau}^*}(C_{\tau}^*|\text{failure types of tests})$$

$$= \exp\left(\ln\left[L(\text{failure types of tests}|C_{\tau}^*)\right] + \kappa\right)$$
(35)

where  $\kappa$  is a normalization parameter so that the cumulative distribution of the posterior sums up to unity. The log-likelihood function is:

$$\ln \left[ L(\text{failure types of tests} | C_{\tau}^*) \right] = \sum_{i=1}^{n_{tot}} Z_i \ln(P_i^*) + (1 - Z_i) \ln(1 - P_i^*)$$
 (36)

$$P_i^* = T(-z_i^*, \text{DOF}) \tag{37}$$

$$z_{i}^{*} = \frac{\hat{C}_{\tau} + \hat{m}_{\tau} \log_{10} \left(\frac{\Delta \tau}{MPa}\right) - \hat{C}_{\sigma} - \hat{m}_{\sigma} \log_{10} \left(\frac{\Delta \sigma/K}{MPa}\right)}{\sqrt{s_{\tau}^{2} (1 + 1/n_{\tau}) + s_{\sigma}^{2} (1 + 1/n_{\sigma})}}$$
(38)

where  $Z_i=1$  or 0 if the test failed in FT3 (fastener shear) or FT1 (ply), respectively, and DOF in Eq. (37) is conservatively taken as the minimum of  $n_\tau-1$  and  $n_\theta-1$ .

## 3. Collected test data

#### 3.1. Fatigue tests of bolts in shear

As mentioned in the introduction, we disregard test series with bolts that failed in FT3, but that had thread in the shear plane [41–43].

Obviously, only tests with snug-tight or semi-prestressed bolts may fail in FT3. Oversized holes may lead to excessive clamping loss during a test [21]. For this reason, we limit our database to tests on fitted bolts and bolts in holes with normal clearance, with the unthreaded shaft in the shear plane, and that failed in FT3. We found only a few tests that satisfied these conditions, since most bearing-type joints and also most pin-lug joints appear to fail in the net section of a plate.

Wichtowski [44] reports a series of 15 specimens with fitted bolts of FT3, tested with a load ratio R=0.1. Fig. 7(a) shows the geometry of the specimens. The M16 bolts were of grade 5.8, with a measured tensile strength of 606 MPa and a minimum yield stress of 420 MPa. They were torqued to 100 N m.

Wilson [16] conducted two test series with bearing-type bolted joints of FT3, one with a load ratio of R=-1 and a geometry according to Fig. 7(b), and one with R=0 and a geometry according to Fig. 7(c). The measured tensile strength and yield stress of the bolts were 834 MPa and 755 MPa, respectively. The specimens according to Fig. 7(b) contained two rivets and two bolts. They were designed such that only the bolts should transfer the shear force. We constructed an FE model of this joint type, which confirmed this hypothesis. Hence, we considered one bolt row in the analytical model;  $n_{row}=1$ .

The total database on bolts contains 27 tests, of which 8 are runouts or tests that failed in FT1, see Table 1. All specimens contain a single (loaded) bolt row. The plate material in all series was tested with mill scale, i.e., without applying a surface treatment to control or enhance the friction coefficient. We do not consider self-loosening of the bolts, i.e., reduction of pretension during the tests [45–47], because the difference in measured prestress at the start and end of Wilson's tests is limited and self-loosening is not reported and also not likely given the test conditions of Wichtowski's tests (fitted bolts, in double covered joints, subjected to pulsating loads, with long lives, hence small displacements).

#### 3.2. Fatigue tests of rivets in shear

Brühwiler [48,49] and Wilson [16] report fatigue test series aimed at rivet shear failure. Wilson [16] reports excessive slip deformations in four of the sixteen tests conducted. Pipinato et al. [17,50] provide four FT3 tests. The systematic study on the influence of joint geometry and stress ratio on fatigue resistance in Graf [13,51] resulted in five FT3 specimens, originating from two series of which two other specimens failed in FT1. Baron and Larson [15], Wilson and Munse [52], and Parola et al. [14] also report test series where some specimens failed in the ply and others in the rivet. Parola's specimens contain rivets with reduced clamping, either by milling off part of the rivet head or by pressing the rivet.

The tests in [51] were conducted in steel grade St37 for the plates and St34 for the rivet material. The Brinell hardnesses of the rivets before and after driving were 128 and 145 kg/mm<sup>2</sup>, respectively, corresponding to approximate ultimate tensile strength of 430 MPa and 480 MPa. Wilson [16] did not report the steel grade, but performed tensile tests on the plates and rivets. The average yield stress and ultimate tensile strength of the steel plates were 242 and 436 MPa, respectively, typical for mild steels around the date of study (1938). The average yield stress and ultimate tensile strength of the carbon steel rivets after driving were 317 and 460 MPa, respectively. These values were 21 and 16% higher than before driving. Parola et al. [14] carried out tests on plates of grade A7-55T with average measured yield stress and ultimate tensile strength values of 289 MPa and 455 MPa, respectively. The rivet yield stress and ultimate tensile strength before driving, according to the mill report, were 204 MPa and 403 MPa, respectively. The tests in Graf [13] were conducted on steel grades equivalent to St52 for the plates and St44 for the rivets, the latter having ultimate tensile strength values between 470 and 520 MPa based on the Brinell hardness. It is unknown whether these data apply before or after driving. The ultimate tensile strength of the ply

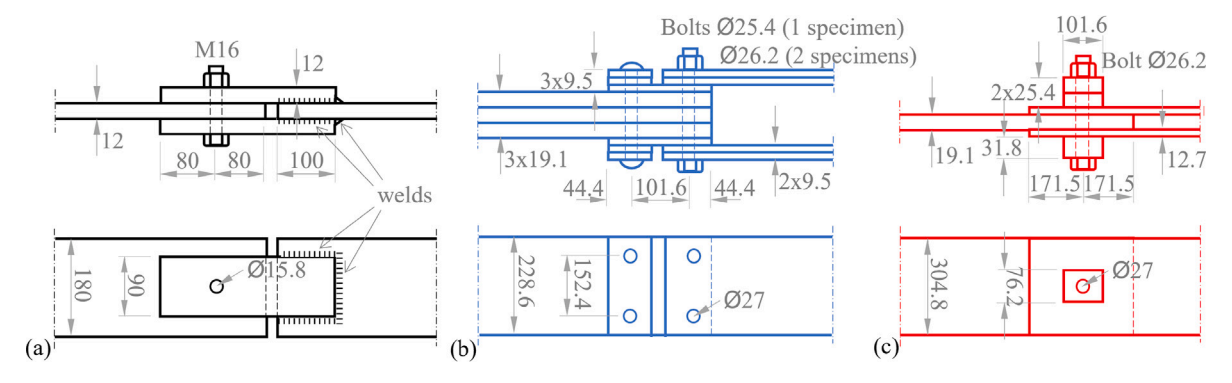


Fig. 7. Lay-out and dimensions (in mm) of bolted joints where bolts failed in FT3: (a) Wichtowski [44], R = 0.1; (b) Wilson [16], R = -1; (c) Wilson [16], R = 0.

Table 1
Test data on bolts of FT3 (without thread in shear plane).

Source	Figure	Holes	$n_{row}$	$n_{pr}$	r [mm]	w [mm]	t <sub>p</sub> [mm]	t <sub>s</sub> [mm]	e <sup>a</sup> [mm]	R	$n_{\tau}$	$n_r$
[44]	7(a)	Fitted	1	1	8	45	6	12	80	0.1	13	2
[16]	<b>7</b> (b)	Normal	1 <sup>b</sup>	2	12.7-13.1	57.3	28.6	28.6	44.4	-1	1	2
[16]	<b>7</b> (c)	Normal	1	1	13.1	152	152	19.1	12.7	0	5	4

<sup>&</sup>lt;sup>a</sup> e = end distance, see Fig. 1.

Table 2
Test data on rivets of FT3 with full geometric information

Source	L,S <sup>a</sup>	$n_{row}$	$n_{pr}$	r [mm]	<i>w</i> [mm]	<i>t<sub>p</sub></i> [mm]	<i>t<sub>s</sub></i> [mm]	p, e <sup>b</sup> [mm]	R	$n_{\tau}$	$n_r$
[13]	S	2	2	10	48	8.5	13	70	-1	2	1
[14]	L	2	2	11.9	52.5	7.2	9.5	105	-1	1	0
[14]	L	2	2	11.9	42.5	9.6	12.2	85	-1	2	0
[15]	L	2	2	10.3	45.2	10.3	13	89	0	2	0
[16]	L	2	2	14.3	57.2	19.1	19.1	101.6	-1	3	0
[16]	S	2	1	14.3	95.3	12.7	15.9	101.6	-1	6	0
[16]	L	1	2	14.3	57.2	9.5	47.6	101.6	-1	0	1
[16]	L	1	2	14.3	57.2	19.1	19.1	101.6	-1	3	0
[16]	L	1°	1 <sup>d</sup>	14.3	57.2	28.6	28.6	101.6	-1	3	0
[51]	S	1	1	10	35	8	10	50	0.02	3	2
[52]	L	1	3	9.5	38.1	12.7	15.9	76	0	2	1

 $<sup>^{</sup>a}$  L = double lap joint, S = double strap joint.

in [15,52] was 436 MPa and 466 MPa, respectively. These sources do not report on the rivet material strength but given the ply strength values, the rivet strength should be similar as in [14,16] and lower than in [51].

The collected database consists of 63 riveted tests, of which 29 riveted double-covered shear joints with full geometric and load information, and 34 riveted tests with incomplete information, some of these conducted on specimens different from double-covered shear joints. Each subset contains five run-outs. Table 2 gives the dimensions of the first subset, where the symbols refer to Fig. 1,  $n_{\tau}$  is the total number of failed tests loaded with the indicated ratio R, and  $n_{r}$  is the number of run-outs, including tests of FT1. Appendix A of the online version of this paper provides a link through which the database can be downloaded.

## 3.3. Clamping stress and friction condition

Application of the analytical model to the test database requires information on the initial clamping stress  $\sigma_{cl,0}$  and the friction coefficient  $\mu$  of the plate faces. Both variables are uncertain. The initial clamping stress of rivets depends on the riveting process [13] and appears to be correlated with the grip [53]. A curve fit of collected experimental data

in [8] provides the following expectation of the clamping stress  $\sigma_{cl,0}$ :

$$\hat{\sigma}_{cl,0} = \frac{265 \text{ MPa}}{\exp\left(\frac{12 \text{ mm}}{h}\right)} \tag{39}$$

The standard deviation of the clamping stress is 35 MPa [53]. We used an expectation of  $\hat{\sigma}_{cl,0}=0$  for Parola's [14] specimens with reduced clamping. This assumption follows from the observation of slip deformations from the onset of load application in [14].

For Wichtowski's [44] bolted joints, assuming an equivalent torquing friction coefficient of 0.15 and using the method in [32], the applied torque of 100 Nm gives an expectation of  $\hat{\sigma}_{cl,0}=160$  MPa.

The expectation of the friction coefficient for mill-scale contact between plates is  $\hat{\mu}=0.33$  and the coefficient of variation is 0.06 [54]. Unless explicitly mentioned, the following sections use the expectations of  $\sigma_{cl,0}$  and  $\mu$ .

## 4. Results and discussion

## 4.1. Stress distribution in the finite element models

We performed more than 200 simulations with the FE method, most of them utilizing a friction coefficient  $\mu=0.3$  and a few additional

<sup>&</sup>lt;sup>b</sup> Only the bolts transfer the force.

<sup>&</sup>lt;sup>b</sup> Column gives pitch p if  $n_{row} > 1$ , or end distance e (see Fig. 1) if  $n_{row} = 1$ .

<sup>&</sup>lt;sup>c</sup> Same geometry as Fig. 7(b), but with bolts replaced by rivets.

<sup>&</sup>lt;sup>d</sup> Only the bolt-replacing rivets transfer the force.

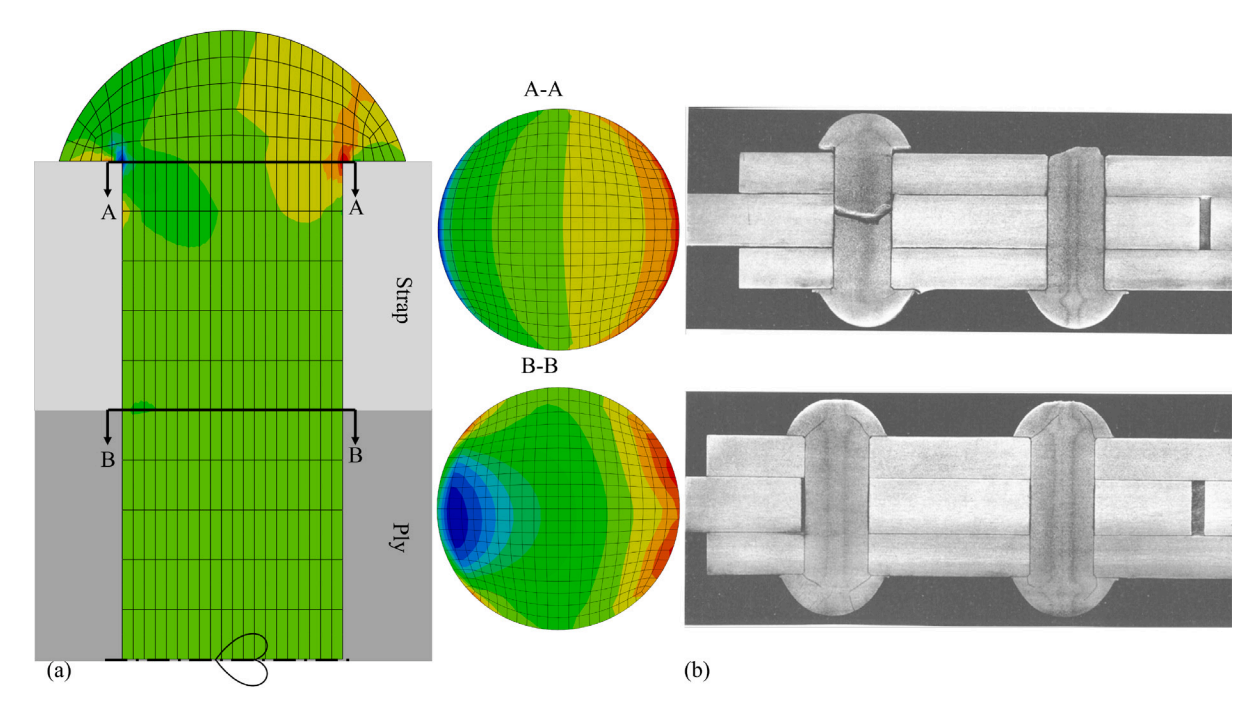


Fig. 8. Shear stress distribution and shear failure location: (a) Prediction of the FE model with maximum absolute shear stress (blue and red contours) at the transition between head and shaft (Section AA) and maximum shear stress range at the shear plane (Section BB — contours re-scaled); (b) Comparison with failures in tests in [13], with cracks initiated at the transition and close to the shear plane (photos copied from [13]).

Table 3
Geometry and load of the simulations of Fig. 9.

Subfigure	$n_{row}$	r/w	$t_p/h$	$t_s/t_p$	$\sigma_{cl,0}$ [MPa]	$\sigma_{net}^{max}$ [MPa]	R
(a)	1	0.24	0.71	1.33	100	66	0
(b)	5	0.24	0.71	1.33	100	198	0
(c)	2	0.16	0.40	1.35	79	119	$^{-1}$
(d)	2	0.23	0.60	1.33	93	91	-1

simulations to check the results with  $\mu=0$ . The simulations reveal two locations of high stress, namely, at the transition between the fastener head and the fastener shaft and in the shear plane; see Fig. 8(a). The former location gives a higher absolute shear stress, whereas the latter location gives a higher shear stress range. These two locations correspond to the fracture locations observed in fatigue tests; see 8(b). However, the shear plane appears to be the dominant failure location — more than 90% of the specimens collected in Section 3 failed at this location, and our analytical model of Section 2.2 therefore considers the shear stress at this location. The shear stress distribution in the shear plane is not uniform. Its maximum is located close to the fastener perimeter; see cross section BB in Fig. 8(a).

Fig. 9 shows some exemplary simulation results with the nominal shear stress according to Eq. (1) in dashed black and the shear stress evaluated with the FE method according to Eq. (2) in solid black as a function of the simulation stages. (The dotted red curves in the figure will be introduced later.) Table 3 provides the geometry and the load condition of the four subfigures. The figure shows discrepancies between the shear stress evaluated with the two equations. The difference increases for a larger number of fastener rows, for which Eq. (1) underestimates the actual shear stress (Fig. 9(b)), and for a larger ratio between the slip force and the applied force, for which Eq. (1) overestimates the actual shear stress, as it does not consider friction (Fig. 9(a)).

## 4.2. Comparison between finite element and analytical models

The dotted red curves in Fig. 9 present the average shear stress range  $\Delta \tau_h$  obtained with the analytical model of Section 2.2. The figure

shows that the model better resembles the average shear stress range derived from the FE method compared to the nominal shear stress range  $\Delta\tau_n$  of Eq. (1). Fig. 10 compares the shear stress range of all FE simulations with the nominal shear stress and the analytical model, in subfigures (a) and (b), respectively. The coefficient of determination of the analytical model  $\Delta\tau_h$  versus  $\Delta\tau_{FE}$  is equal to  $R_{sq}=0.99$ — an improvement over  $R_{sq}=0.94$  for the nominal shear stress  $\Delta\tau_n$  of Eq. (1). The ratio  $\Delta\tau_h/\Delta\tau_{FE}$  has a mean of 0.94 and the standard deviation is 0.08. For reference, the mean and standard deviation of  $\Delta\tau_n/\Delta\tau_{FE}$  are 1.41 and 0.37, respectively.

# 4.3. S-N curves for bolts in shear

Fig. 11(a) shows the fatigue test data of the bolts with FT3 using the nominal shear stress of Eq. (1). The series colors match those of the specimen geometries in Fig. 7. The estimates of the slope parameters of the S–N curve of the black and red series ( $R \approx 0$  for both series) differ significantly:  $\hat{m}_{\tau} = -8.0$  and  $\hat{m}_{\tau} = -1.4$ , respectively. The runouts of the blue series (R = -1) are in disagreement with the failed specimen, suggesting an extremely large scatter if the nominal shear stress is considered as the fatigue driving force. The red series shows similar disagreement between run-outs and failed specimens with the lowest applied stress range.

Fig. 11(b) shows the same data, but using the average shear stress range according to the analytical model, Eq. (4). The standard deviation of the S–N curve,  $s_{\tau}$  — Eq. (23), reduces from 0.35 for  $\Delta \tau_n$  to 0.29 for  $\Delta \tau_h$ . The shear stress ranges of the specimens resulting in run-outs are now lower than those of the failed specimens for the individual series, in line with expectations. The slope parameters of the S–N curves of the black and red series are also better aligned, although the difference remains significant:  $\hat{m}_{\tau} = -5.4$  and  $\hat{m}_{\tau} = -1.9$ , respectively. The fatigue resistance of the red series is higher than that of the black series. The difference in tensile strength is an unlikely reason for this difference, because the bolts are subjected to a high notch effect due to the concentrated load application in the shear plane. This concentrated load is also responsible for the stress concentration in the bolt, see Fig. 9(a) cross-section BB. It is known that the influence of tensile

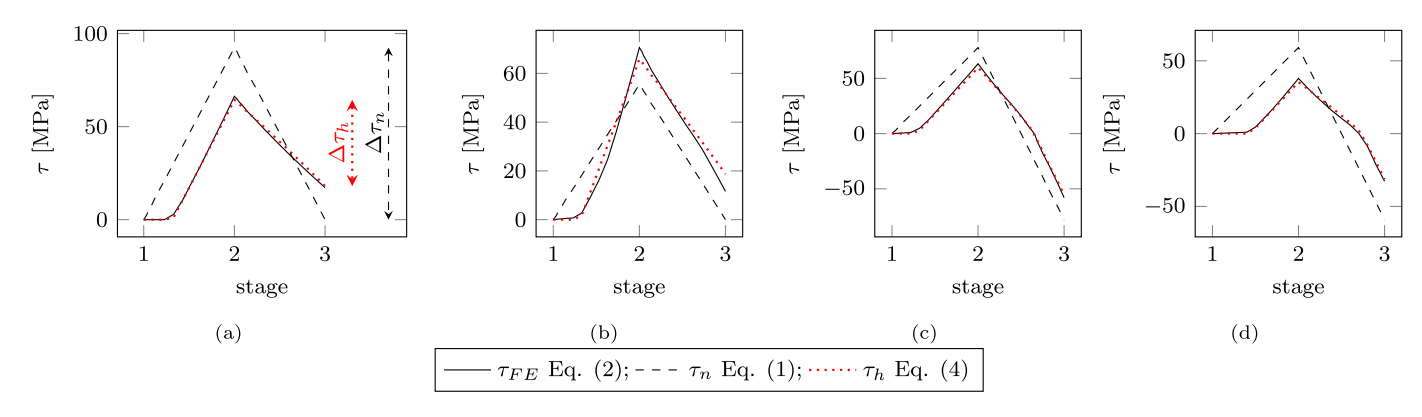


Fig. 9. Exemplary simulations of the average shear stress per shear plane with  $\mu = 0.3$  (geometry and load according to Table 3). The nominal shear stress range of Eq. (1) does not match the FE result. The analytical model of Section 2.2 (Eq. (4)) gives a better estimate.

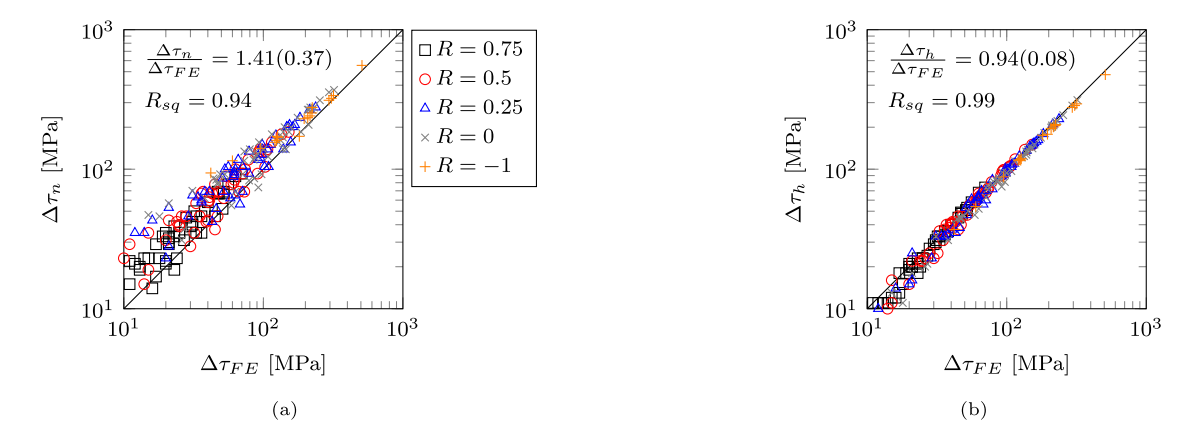


Fig. 10. Comparison between the average shear stress of the FE simulations and analytically derived estimates: (a)  $\Delta \tau_n$ , Eq. (1); (b)  $\Delta \tau_h$ , Eq. (4). The estimate of Eq. (4) agrees better with the FE simulations than that of Eq. (1).

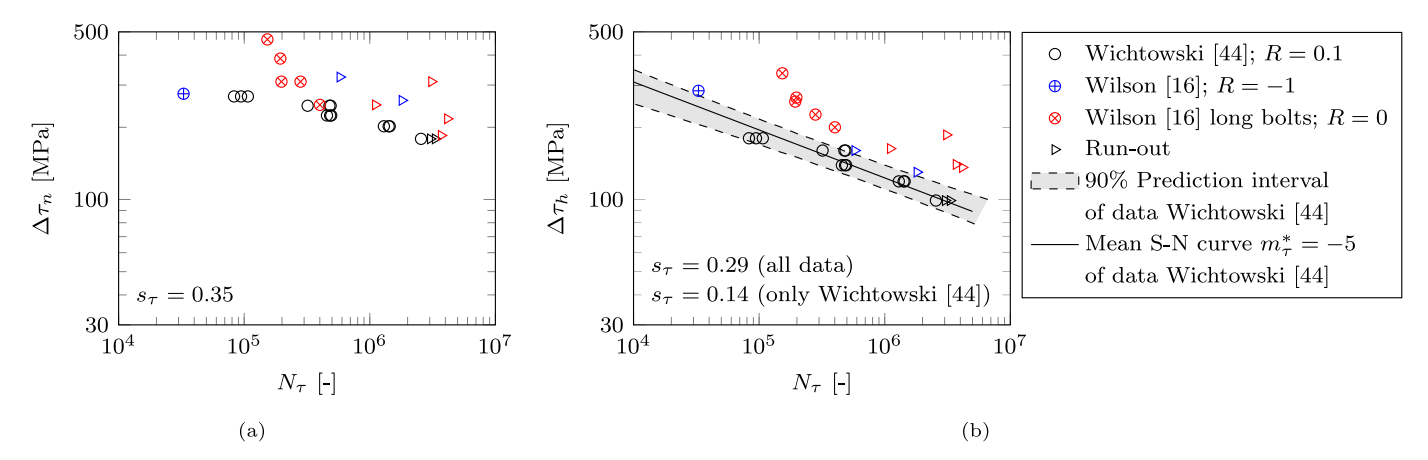


Fig. 11. Fatigue test data of bolts failing in shear: (a) Using the nominal shear stress  $\Delta \tau_n$  (Eq. (1)), showing large scatter; (b) Using the average shear stress  $\Delta \tau_h$  (Eq. (4)), showing reduced scatter;.

strength is small for severely notched components [55]. We also do not expect the difference in hole filling between fitted bolts (black series) and normal clearance holes (red series) to be the cause of the difference in fatigue performance. Parola et al. [14] expect a lower stress concentration and therefore a better fatigue performance for fitted fasteners, but White [56] shows a higher fatigue resistance of the lug for both clearance fit pins (red series) and interference fit pins (black series) compared to pins with a radius equal to the radius of the lug. An alternative explanation is as follows. The distance between the bolt head or nut and the shear planes is large relative to the bolt radius for the red series (see Fig. 7). These bolts are therefore subject to a

significant bending moment if the joint is loaded. A FE model made of this joint reveals that the bending moment developed at the load levels applied in the tests results in a compression stress at the location of maximum shear stress in the shear plane, despite of the bolt prestress. A compression stress in combination with a cyclic shear stress postpones fatigue crack initiation [57] and reduces the crack propagation rate [58] compared to the case without compression. This may explain the higher fatigue resistance. Because of their unusual configuration, we have disregarded the red series and have only considered the black series in the regression analysis of the tests with pulsating load ( $R \approx 0$ ).

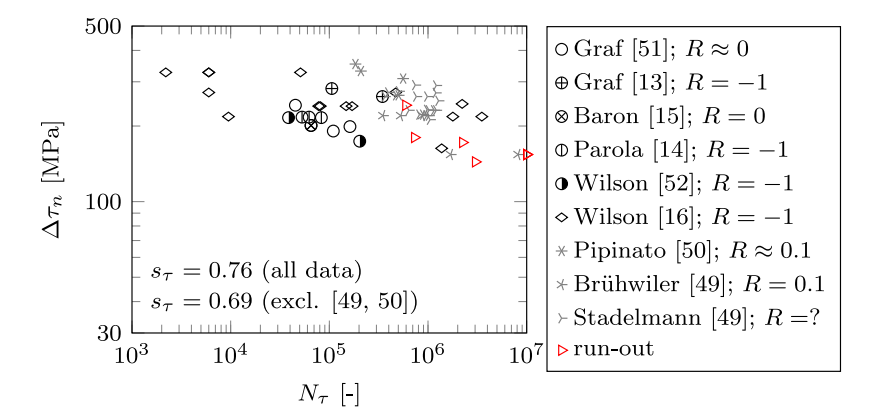


Fig. 12. Fatigue test data of hot rivets failed in shear, using the nominal shear stress. The data show a very large scatter.

The standard deviation of the black series is relatively small:  $s_{\tau}=0.14$ . The 90% confidence interval of  $m_{\tau}$  resulting from Eq. (25) is  $-4.6 < m_{\tau} < -6.3$  and the estimate is  $\hat{m_{\tau}}=-5.4$ . Specifying a predefined slope of  $m_{\tau}^*=-5$  for design purposes, the characteristic reference fatigue resistance for the shear stress according to the analytical model is  $\Delta\tau_C=96$  MPa. To date, the standards EN 1992-1-9 [18] and BS 7608 [19] and the guideline DNV-RP-C203 [20] use the nominal shear stress of Eq. (1) for evaluating the fatigue resistance. For the special case of a joint with one bolt row without prestress, the nominal shear stress equals the average shear stress according to the analytical model. For this case, the standards provide a characteristic reference fatigue resistance of  $\Delta\tau_C=100$  MPa, i.e., in line with the regression applied here.

Fatigue tests on plain material loaded in shear or torsion show only a small influence of the mean shear stress on the fatigue resistance [59]. However, the blue series, conducted with a fully reversed load, provides a larger resistance compared to the black series, conducted with a pulsating load. A similar influence of the load ratio will be shown below for rivets. This influence is probably related to the fact that the stress concentration in the shear plane at the advancing side of the bolt is higher than that at the retreating side. The advancing and retreating sides change between tension and compression in reversed loading, implying that the stress concentration during the first semi cycle is different from that during the second semi cycle. Note that  $\Delta\tau_h$  depends on the mean stress.

Consideration of the slip force in the tests was necessary to derive the S–N curves. For applying the curves, care should be taken to prevent the bolt from loosing if relying on slip force; it is safe-sided to ignore a slip force.

## 4.4. S-N curves for rivets in shear

Fig. 12 presents the fatigue test data of the riveted joints of FT3 as a function of the nominal shear stress  $\Delta \tau_n$ . The standard deviation,  $s_\tau = 0.76$ , is extremely large compared to other structural details with mechanical fasteners [7,60]. This standard deviation ignores run-outs. Similarly to bolts, the run-outs and the failed data disagree, resulting in an even larger standard deviation, had this been accounted for.

Fig. 13(a) presents the rivet data of which the geometry is known (allowing for application of the analytical model) using the average shear stress range of the analytical model,  $\Delta \tau_h$ . The standard deviation,  $s_\tau=0.65$ , has slightly reduced compared to the nominal shear stress range (Fig. 12,  $s_\tau=0.69$  for the same data), but it is still excessively large. Four tests stand out in Fig. 13(a) with a very low resistance. Wilson [16] reports large slip deformations for exactly these four tests. Large slip implies ineffective clamping. Moreover, the friction coefficient changes when slip occurs [61–63]. For these reasons, we also evaluated these four tests with zero slip force ( $\sigma_{cl,0}=0$ ), resulting in the arrow tips in Fig. 13(b). The arrow tips are within the 90% confidence

interval of the other tests. It should also be mentioned that the provided shear stress of three out of these four tests in [16] — shown in blue in Fig. 13(b) – does not agree with the net section stress reported in the same source. Hence, these data are uncertain. In addition, three of the tests in [16] failed at or before  $N_{\tau} < 10^4$ , often considered the division between low and high cycle fatigue. The standard deviation reduces to  $s_{\tau} = 0.26$  using  $\Delta \tau_h$  if all data from Wilson [16] are excluded.

To demonstrate the influence of the uncertainty in clamping stress and friction coefficient, the whiskers in Fig. 13(b) represent the 50% confidence interval of the shear stress range per test. We determined these intervals by performing Monte Carlo simulations with the model of Section 2.2, using the expectations and standard deviations of  $\sigma_{cl,0}$  and  $\mu$  mentioned in Section 3.3. The figure shows a significant, test-dependent, effect of the slip force uncertainty on the average shear stress  $\Delta \tau_h$ . The uncertainty in the S–N curve can be reduced by performing fatigue tests on geometries with red lead paint on the plate faces, which significantly reduces the friction coefficient  $\mu$  [54]. We have not found such tests with FT3 in the literature.

Fig. 14(a) provides the FT3 test data of rivets subjected to a fully reversed load (R=-1), excluding Wilson's data [16]. This subset has a low standard deviation of  $s_{\tau}=0.09$ . The 90% confidence interval of the slope parameter is  $-8.6 < m_{\tau} < -4.0$ , with an expectation of  $\hat{m}_{\tau}=-6.3$ . Therefore, a predefined slope of  $m_{\tau}^*=-5$  seems reasonable. The corresponding characteristic fatigue resistance is 99 MPa. However, the S–N curve is based on no more than  $n_{\tau}=5$  test data. Therefore, we compare the 90% prediction interval with that of the bolts of Fig. 11(b) (R=0.1), see the blue-hatched areas in Fig. 14(a). The prediction interval of the rivets is slightly wider than that of the bolts, which is caused by the limited number of tests available in the subset of rivets with R=-1. Ignoring this, the prediction intervals agree well — slightly higher for the rivets, which is in line with the difference in stress ratio.

Fig. 14(b) provides similar data, but for a pulsating load. These fatigue test data are in disagreement with the other subsets (rivets with R = -1 and bolts); the S–N curve is lower and has a steeper slope. A certain deviation between subsets is possible regarding the differences in stress concentration and material, but the difference is larger than expected. A possible reason is the relatively high stress to which the rivets are exposed in this subset. The combination of shear stress due to external load and normal stress due to clamping causes a von Mises stress that is on average 324 MPa for failed tests in the subset, whereas the reported yield stress of rivets of similar grades is between 204 MPa and 317 MPa (Section 3). Thus, the rivets have yielded. Evaluations with most of the common mean stress correction factors for tension, summarized in [64], and the collected data for shear in [59], show that only a small effect of yielding is expected on the fatigue resistance for pulsating load, provided that the maximum stress remains well below the tensile strength. However, yielding of the rivet can relax the clamping stress, resulting in a reduced or negligible slip force. For

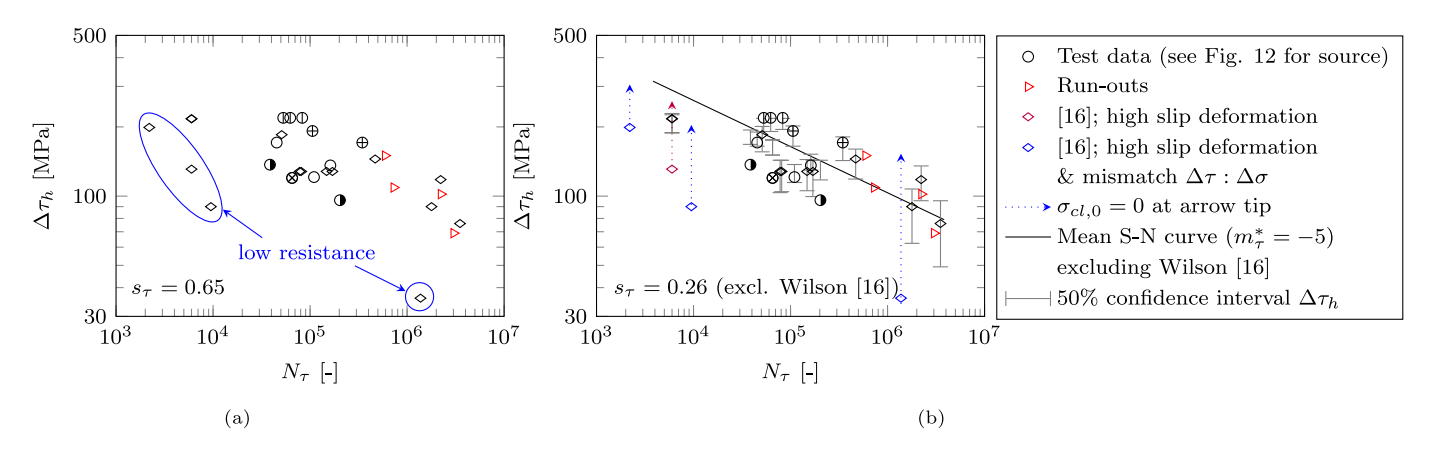
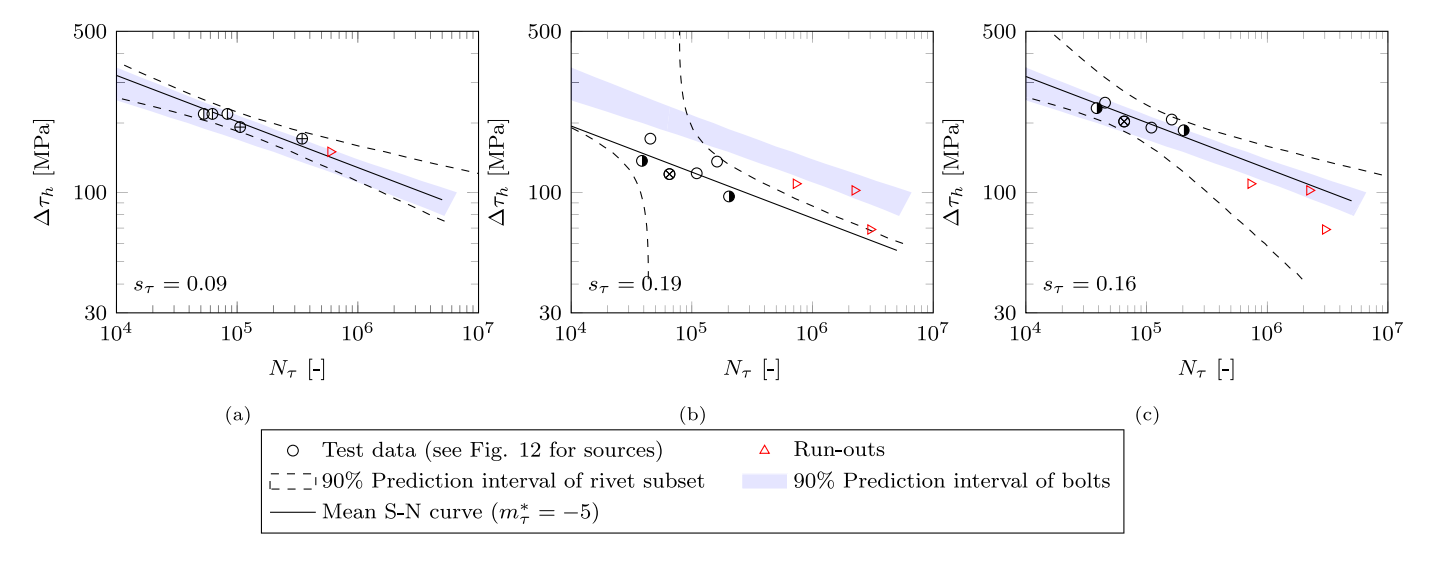


Fig. 13. Fatigue test data of hot rivets that failed in shear, using the modified shear stress: (a) Highlighting the four outliers of Wilson [16], for which large slip was reported from the onset of the tests; (b) Analysis with  $\sigma_{el,0} = 0$  for the four tests in [16] and the 50% confidence interval for other tests.



**Fig. 14.** S–N curves for hot rivets that failed in shear, using  $\Delta \tau_h$ : (a) Fully reversed load (R = -1), S–N curve in good agreement with bolts with R = 0.1; (b) Pulsating load ( $R \approx 0$ ), S–N curve much lower than bolts with R = 0.1; (c) Pulsating load assuming no clamping due to rivet yielding, S–N curve in good agreement with bolts with R = 0.1.

this reason, Fig. 14(c) provides the same data, but assuming absence of clamping for the failed tests. The test results using this assumption agree well with that of the rivets with R=-1 and the bolts with R=0.1. The standard deviation is  $s_{\tau}=0.16$ , the expectation of the slope parameter is  $\hat{m}_{\tau}=-5.0$ , and the characteristic reference fatigue resistance is  $\Delta \tau_C=95$  MPa. The prediction interval is relatively wide, due to the limited number of tests and the limited difference in the average shear stress range between the tests.

Note that three of the tests with R = -1 in Fig. 14(a) were carried out with reduced clamping, where the slip force was assumed absent, and the other two tests had a lower von Mises stress in the rivets (209 MPa) and a higher steel grade of the rivets (St44). This is the reason why we did not adjust the clamping stress for these tests. Similarly, the Von Mises stress remained below the yield stress in Wichtowski's bolts [44].

Because of the small number of available tests and the uncertainty in slip force, the next section evaluates the S–N curves for FT3 with the test data of FT1.

## 4.5. Updated S-N curves for rivets using ply failure data of riveted joints

The number of available fatigue test data of rivets in FT3 is limited. Many more data are available on riveted joints in FT1. Eq. (32) allows us to evaluate if the S–N curves derived in the previous section, together with the S–N curves for FT1, can correctly predict the failure type.

The number of tests on carbon steel specimens with FT1 collected in [8] with R = -1 is 58. The estimators of the S-N curve are  $m_{\sigma} =$ -4.24,  $\hat{C}_{\sigma} = 15.112$ , and  $s_{\sigma} = 0.235$ . Fig. 15(a) presents the ratio between the average shear stress range and the hoop stress range for the tests with R = -1. The solid black curve represents the expectation of the division between FT1 and FT3, obtained using Eq. (32) with P = 0.5 and the S-N curves mentioned above. The different slopes of the S-N curves cause the division to curve. We expect specimens with  $K\Delta\tau_h/\Delta\sigma_h$  smaller and larger than this division to fail in FT1 and FT3, respectively. The hashed area represents the 90% confidence interval of the division. Blue ○ and red ⊗ symbols represent tests that failed in FT1 and FT3, respectively. For reference, the figure also displays the rivet test data of Wilson [16] with orange  $\oplus$  symbols. All tests except for one show a failure type in agreement with the division. The exception test was one of a twin with exactly the same geometry and applied load. One of the twin specimens failed in the rivet (in agreement with the division) and the other failed in the ply (in disagreement). None of the other tests failed in a type different from predicted.

The number of tests on carbon steel specimens with FT1 collected in [8] with pulsating load, for which we considered tests with  $0 \le R \le 0.2$ , is 379. The estimators of the S–N curve are  $m_\sigma = -3.76$ ,  $\hat{C}_\sigma = 14.206$ , and  $s_\sigma = 0.327$ . Fig. 15(b) presents the test data and the division assuming rivet clamping, i.e., the S–N curve of Fig. 14(b) that disregards yielding of the rivets. The figure shows that many tests failing in FT1 are predicted to fail in FT3. Given the high level of

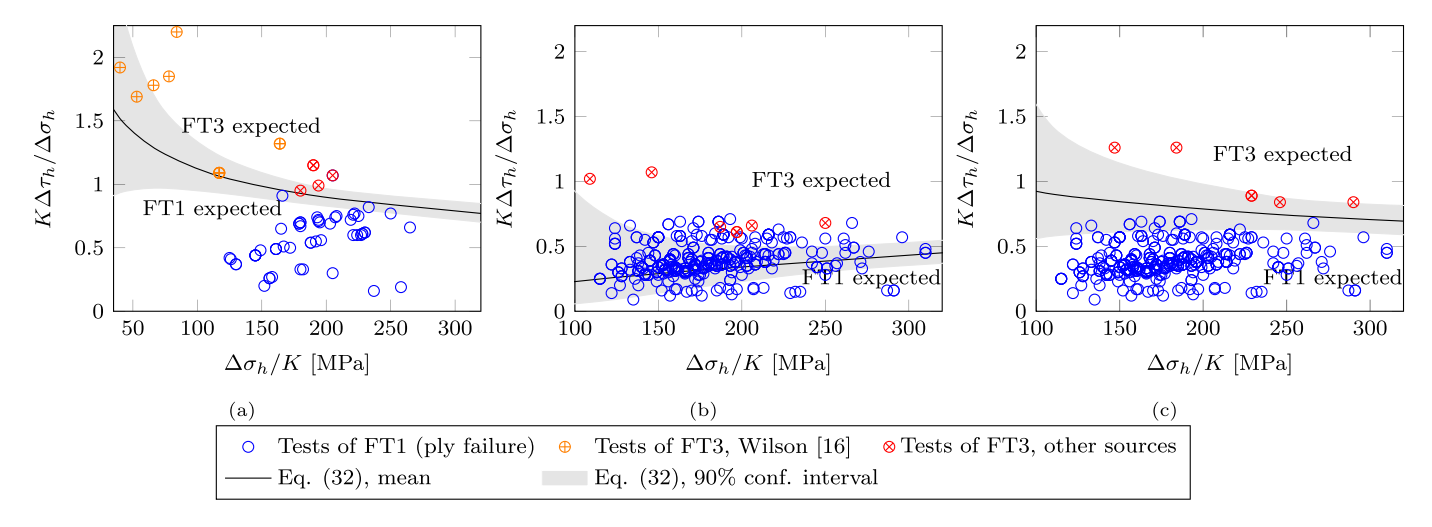


Fig. 15. Expectation of the failure type based on the S–N curves, Eq. (32), and actual test data: (a) Fully reversed (R = -1), tested failure types in agreement with prediction; (b) Pulsating ( $0 \le R \le 0.2$ ) disregarding rivet yielding, tested failure types in disagreement with prediction; (c) Pulsating ( $0 \le R \le 0.2$ ) assuming  $\sigma_{cl,0} = 0$  for rivets that have yielded, tested failure types in agreement with prediction.

confidence in the S–N curve for FT1, as it is based on many test data, this result indicates that the S–N curve for FT3 and pulsating load, as obtained with Fig. 14(b), is too low. Fig. 15(c) uses the same data ( $R\approx 0$ ) but assuming absence of clamping because of rivet yielding (S–N curve of Fig. 14(c)). With this assumption, all test data failed according to the prediction. This provides additional confidence in the S–N curve of Fig. 14(c).

## 4.6. Summary of S-N curves

Fig. 16 combines all FT3 test data in one S–N plot, but excluding Wilson's [16] data on bolts, because of the non-standard dimensions (Section 4.3) and on rivets, as we have reason to question the reliability of these data (Section 4.4). The plot uses the shear stress according to the analytical model. In line with the prediction of the failure type, the tests in which yielding of the rivets is expected are evaluated without clamping. A small scatter results, with a standard deviation  $s_{\tau} = 0.15$ . The characteristic reference fatigue resistance is  $\Delta \tau_C = 97$  MPa.

Fig. 17 provides the distribution of  $C_{\tau}^*$  as determined from Bayesian inference using the failure types, Eq. (35), and the shear stress according to the analytical model. The expectation of  $C^*_{\tau}$  according to this analysis is slightly higher for the subset of rivets with R = -1compared to the subset of rivets with  $R \approx 0$ , the latter considered without clamping. A similar observation of slightly higher resistance for fully reversed load applies to bolts, see Section 4.3, which we explained by a change in location of the maximum stress concentration between tension and compression. The standard deviations of  $C_{\pi}^*$  of these two subsets are similar. The standard deviation is lower if all data (excluding Wilson's [16]) are combined, mainly because of the larger number of data. The expectation is also slightly lower if all data are combined, mainly because of the lower ratio  $K\Delta\tau_h/\Delta\sigma_h$  of Wichtowski's bolt data compared to the rivet data. The 95% exceedance fraction of  $C^*_{\tau}$  follows from the cumulative distribution  $F_{C_{\tau}}$ , see the insert in Fig. 17(b), which also gives the resulting values of  $\Delta \tau_C$ .  $C_{\tau}^*$  is Gaussian distributed, allowing us to determine  $\hat{C}_{\tau}^*$  and  $s_{\tau}^*$  from a least squares fit of the curves.

Tables 4 and 5 provide the resulting parameters of the S–N curve for all subsets using a free slope and a predefined slope, respectively. The latter tables use the regression analyses of the FT3 tests, as well as the Bayesian inference procedure of the failure types. The final column of each table provides the log-likelihood according to Eq. (36). The gray rows provide the rivets with R=0 assuming full clamping, i.e., without considering yielding of the rivets. In line with the observations above, this analysis gives a much lower log-likelihood than for the assumption

without clamping, and the characteristic reference fatigue resistance is also unexpectedly low and out of range of the other test data. For the other analyses, the log-likelihoods of the regression are similar to those of the Bayesian inference. The characteristic reference fatigue resistance values are also similar. These are slightly below 100 MPa for the regression analyses (95 MPa  $\leq \Delta \tau_C \leq$  99 MPa) and slightly above 100 MPa for the Bayesian inference (108 MPa  $\leq \Delta \tau_C \leq$  118 MPa). A characteristic reference fatigue resistance of  $\Delta \tau_C =$  100 MPa seems therefore a reasonable choice for assessments.

## 4.7. Geometries sensitive for fastener failure

Eq. (32) and the S-N curves of the previous section allow studying geometries and load conditions of double covered riveted joints for which FT3 is decisive. We consider the expectations of the fatigue resistance of both types of failure, where we assume S-N curves with a predefined slope of  $m_{\tau}^* = -5$  and  $m_{\sigma}^* = -5$ . The corresponding expectations of the intercept parameter are  $C_{\tau}^* = 16.49$  and  $C_{\sigma}^* = 16.96$ . Fig. 18 provides the results, where the axes provide the geometry parameters (see Fig. 1 for the symbol explanation) and the curves provide the division between FT1, decisive for geometries below the curve, and FT3 decisive above the curves. The curves should be considered as indicative, because the parameters of the S-N curve are expectations, with the remaining uncertainty for FT3, and we made a choice for the predefined slope. Hence, joints with geometries relatively close to the division curves may fail in a mode different from predicted. The curves with zero slip force apply if clamping cannot be guaranteed or if the friction coefficient might be low. Examples of the former are loose rivets detected in inspections or rivets that may have yielded under service loads. An example of the latter is a joint in which (red lead) paint is applied on the plate faces, because other studies consistently report a low friction coefficient between plates shortly after application of red lead paint, with  $\hat{\mu} = 0.06$  [54], whereas it is uncertain in the long term, reported between similar to shortly after application [65] up to  $\hat{\mu} = 0.27$  [66]. The applied load relative to the clamping stress has a moderate influence on the results for a non-zero slip force. The results in Fig. 18 apply for  $\sigma_{net} = 150$  MPa and the expectation of the clamping stress with a rivet grip equal to twice the ply thickness, i.e.,  $t_n = t_s$ . As an indication, for the cases with clamping and friction, the division curves are on average 5% higher than displayed for  $t_s = 2t_n$ and 8% lower than displayed for  $\Delta \sigma_{net} = 200$  MPa. The figure applies to riveted double-covered shear joints, where the fasteners are hole filling. However, we expect similar trends for double-covered shear joints with snug-tight bolts in normal clearance holes.

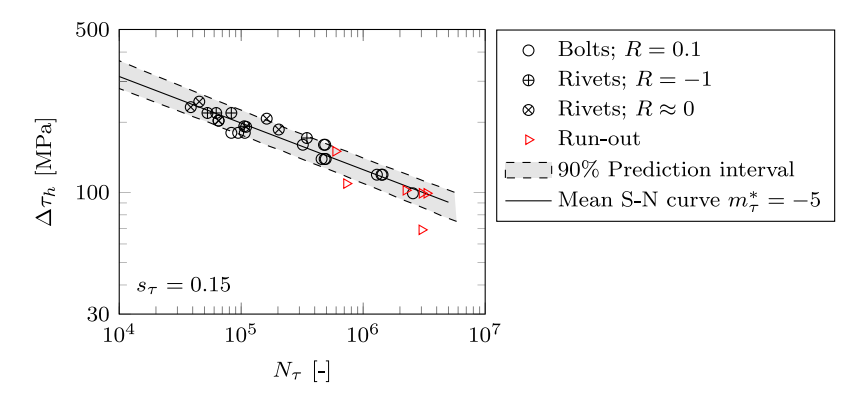


Fig. 16. S-N curves of all tests of FT3, excluding Wilson's tests [16], and assuming no clamping if the fastener could have yielded.

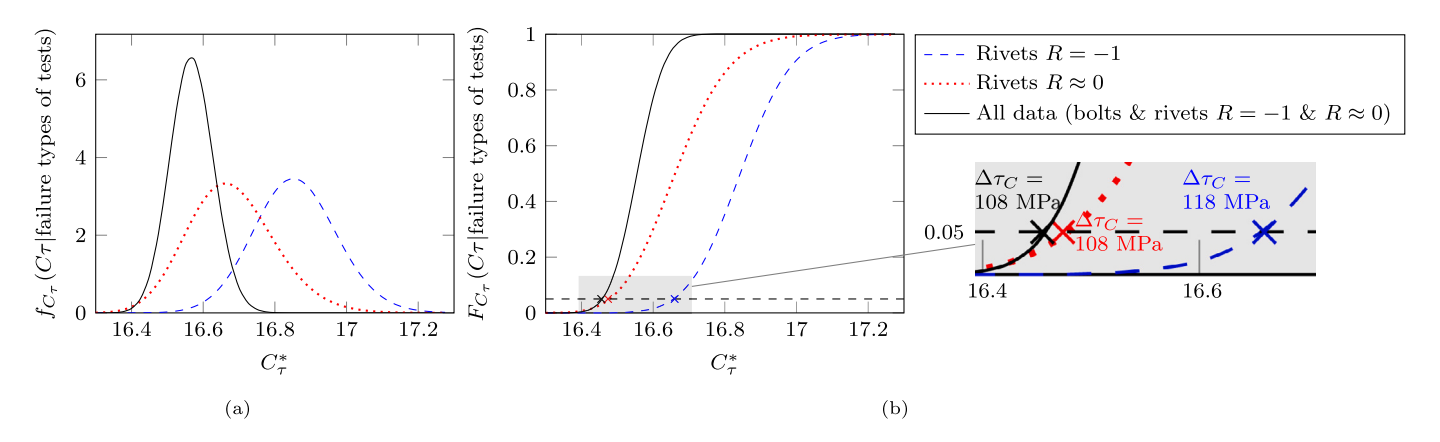


Fig. 17. Parameter  $C_r^*$  determined from the Bayesian inference (Eq. (35)) using the failure types of all tests, and assuming no clamping if the fastener could have yielded: (a) Probability density; (b) Cumulative distribution.

Table 4 S–N curve parameters for FT3 using a free slope, excluding Wilson's [16] tests on bolts and rivets, based on  $\Delta \tau_h$ .

Detail & load ratio	Basis S–N curve	$\hat{m}_{ au}$	$\hat{C}_{\tau}$	$s_{\tau}$	ln(L) Eq. (36)
Bolts $R \approx 0$	Fig. 11(b)	-5.45	17.43	0.14	_
Rivets $R = -1$	Fig. 14(a)	-6.32	19.59	0.09	-9
Rivets $R = 0$	Fig. 14(b) <sup>a</sup>	-2.35	9.87	0.19	-445
	Fig. 14(c) <sup>b</sup>	-5.01	16.55	0.16	-26
All data <sup>b</sup> & all load ratios	Figs. 11(b) & 14(a&c)	-4.91	16.29	0.15	-34

<sup>&</sup>lt;sup>a</sup> Assuming clamping.

Table 5 S-N curve parameters for FT3 using a predefined slope  $m_{\tau}^* = -5$ , excluding Wilson's [16] tests on bolts and rivets, based on  $\Delta \tau_h$ .

Detail & load ratio	Basis S–N curve	$\hat{C}^*_{ au}$	$S_{\tau}^{*}$	$\Delta  au_C$ [MPa]	ln(L) Eq. (36)
Bolts $R \approx 0$	Regression, Fig. 11(b)	16.45	0.15	95	_
Rivets $R = -1$	Regression, Fig. 14(a) Bayesian, Eq. (35)	16.54 16.85	0.11 0.12	99 118	-11 -7
Rivets $R = 0$	Regression, Fig. 14(b) <sup>a</sup> Regression, Fig. 14(c) <sup>b</sup> Bayesian, Eq. (35) <sup>b</sup>	15.44 16.52 16.67	0.27 0.16 0.12	52 95 108	-174 -29 -15
All data <sup>b</sup> & all load ratios	Regr. Figs. 11(b) & 14(a&c) Bayesian Eq. (35)	16.49 16.57	0.15 0.06	97 108	-31 -30

<sup>&</sup>lt;sup>a</sup> Assuming clamping.

Fig. 18 shows that the joints are more prone to FT3 instead of FT1 for:

- $\bullet$  Thicker plates, relative to the plate width.
- · Lower slip force.
- · Lower mean stress.

- · Smaller number of rivet rows.
- · Larger plate widths per rivet, relative to the hole radius.

<sup>&</sup>lt;sup>b</sup> Assuming no clamping for rivets with R = 0 (series where rivets have yielded).

<sup>&</sup>lt;sup>b</sup> Assuming no clamping for rivets with R = 0 (series where rivets have yielded).

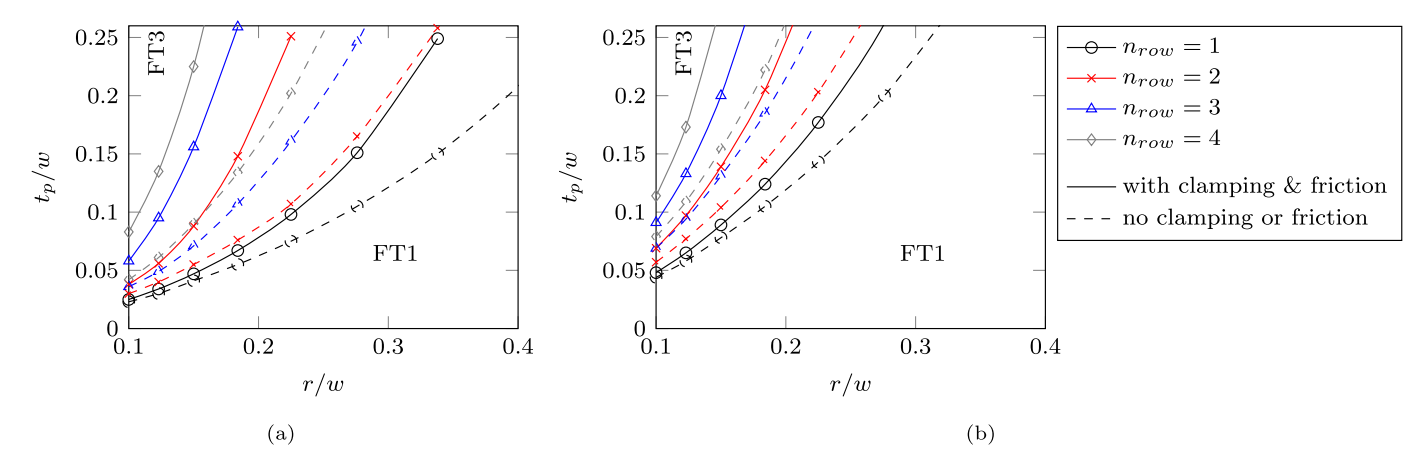


Fig. 18. Geometric division between FT1 and FT3. FT3 is expected for geometries above the curves: (a) Fully reversed load R = -1; (b) Pulsating load R = 0.

The first three items imply that joints with few rivets having relatively small shaft radii are sensitive to FT3. In such joints, both the hoop stress range in the ply  $\Delta\sigma_h$ , and the shear stress range in the fastener  $\Delta\tau_h$ , are high compared to the net section stress range,  $\Delta\sigma_{net}$ , but  $\Delta\tau_h$  is more sensitive to these geometric variations. With respect to mean stress, we expect that FT3 is decisive for all joints subjected to cyclic compression, because the plates are not prone to fatigue failure in that case. For cyclic tension loads with R>0, both  $\Delta\sigma_h$  and  $\Delta\tau_h$  increase compared to R=0, but  $\Delta\sigma_h$  is more dependent on the mean stress.

Joints with geometries above the curves in Fig. 18, for which FT3 is expected, are not the most common. This partially explains why more than 90% of the collected fatigue test data failed in FT1 instead of FT3. However, this is also due to practical test conditions, because the specimens and the load need to be relatively large to induce FT3 (small r/w, small  $r/t_p$ , implies a large ply cross section for a given rivet radius). The tests collected and the evaluations in this paper demonstrate that FT3 cannot be excluded for all double-covered joints. In addition, the tests in [17,49] show that FT3 can be decisive in other types of riveted joints, such as in truss girders or beams composed of plates and angle sections.

To evaluate whether the nominal shear stress range  $\Delta \tau_n$  according to Eq. (1) can be applied to assess fatigue resistance, despite its shortcomings, we evaluate the ratio between  $\Delta \tau_n$  and  $\Delta \tau_h$  for geometries on the curves, i.e., for which FT3 is equally likely than FT1. This ratio is  $0.90 \le \Delta \tau_n / \Delta \tau_h \le 1.1$  for zero slip force and  $1.1 \le \Delta \tau_n / \Delta \tau_h \le 2.3$  for nonzero slip force. Slightly higher ratios result for geometries above the curves. The large difference between the two shear stress ranges, and the large scatter of the test data if evaluated with  $\Delta \tau_n$ , demonstrate that the nominal shear stress range is not a good indicator of its fatigue performance. A lower bound fatigue resistance for double-covered joints based on  $\Delta \tau_n$ , which can be excessively conservative, results by multiplying  $\Delta \tau_C = 100$  MPa as derived for  $\Delta \tau_h$  with the lowest value of  $\Delta \tau_n / \Delta \tau_h$ . This gives a characteristic reference fatigue resistance of 100 MPa  $\cdot$  0.90 = 90 MPa. We conclude that the characteristic reference fatigue resistance of 140 MPa for  $\Delta \tau_n$  as proposed by [11], and based on the tests in [49], see [67], could suffice for specific geometries, but is too high for the general case.

## 5. Conclusions

This paper concerns fatigue failure of fasteners in double-covered shear joints with rivets or with snug tight bolts. Using the finite element method and available test data, we demonstrate that the nominal shear stress in the fastener is not a good indicator of fatigue performance. We derive a set of equations that approximate the average shear stress per shear plane, which we call the analytical model. The model agrees well with 200 finite element simulations; the coefficient of determination between the analytical model and the finite element simulations is 0.99.

The application of the analytical model requires an S–N curve derived from tests. We found a limited number of tests that failed in the fastener in the literature. This limited number, together with the scatter of the fastener clamping stress and the friction coefficient, causes the derived S–N curve to be uncertain. However, the selected S–N curve appears to be consistent with the prediction of the failure mode, which enhances confidence in the S–N curve. Using a predefined slope parameter of  $m_{\tau}^* = -5$ , the characteristic reference fatigue resistance for the shear stress range according to the analytical model is approximately  $\tau_C = 100$  MPa, that is, slightly lower for the regression of the fastener failure test data, and slightly higher for the Bayesian inference using the failure types of the test.

The evaluations in this paper show that double-covered shear joints are more sensitive to fatigue failure of the fasteners in shear, instead of net section failure of the ply, if the number of fasteners and the dimensions of the fasteners are relatively small (small number of fastener rows, large ratio of plate width over fastener radius, and large ratio of plate thickness over fastener radius), if the mean load of the cycle is low, and/or if the force transferred through friction is low (low clamping stress or paint on the plate faces). Fig. 18 provides the failure mode division for the combination of parameters. Most practical joints have dimensions for which failure of the ply is decisive. However, failure of a fastener is expected to be the only (and hence dominant) fatigue failure type for a joint subjected to cyclic compression.

Yielding of the fasteners under service loads should be checked, because the evaluation of the fatigue tests suggests that a slip force cannot be relied on in such a case. However, more tests are required to confirm this hypothesis.

## CRediT authorship contribution statement

**Johan Maljaars:** Writing – original draft, Methodology, Investigation, Formal analysis, Data curation, Conceptualization. **Sjoerd Hengeveld:** Writing – review & editing, Investigation. **Jorrit Rodenburg:** Writing – review & editing, Investigation.

# Declaration of competing interest

The authors declare the following financial interests/personal relationships which may be considered as potential competing interests: Johan Maljaars reports financial support was provided by Office for Public Works and Water Management Infrastructure division. If there are other authors, they declare that they have no known competing financial interests or personal relationships that could have appeared to influence the work reported in this paper.

#### Acknowledgments

We thank the Dutch asset owner of road bridges Rijkswaterstaat for sponsoring this study.

## Appendix A. Supplementary data

RivetEval.xlsm is a MS Excel sheet that includes the database and all equations of the analytical models.

Supplementary material related to this article can be found online at https://doi.org/10.1016/j.ijfatigue.2025.108929.

#### Data availability

The supplementary material including the data and the code is also available at: https://publications.tno.nl/publication/34643949/YeWIHjAo/maljaars-2025-RivetEval.xlsm.

#### References

- [1] Imam Boulent M, Righiniotis Timothy D. Fatigue evaluation of riveted railway bridges through global and local analysis. J Constr Steel Res 2010;66:1411–21.
- [2] Jia Donglin, Zhang Qinghua, Xiong Lvbo, Li Jun, Bu Yizhi, Bao Yi. A unified evaluation method for fatigue resistance of riveted joints based on structural stress approach. Int J Fatigue 2022;160:106871.
- [3] Horas Cláudio S, Silva João N, Correia José AFO, De Jesus Abílio MP. Fatigue damage assessment on aging riveted metallic railway bridges: A literature review. Structures 2023;58:105664.
- [4] Collette Quentin. Riveted connections in historical metal structures (1840-1940). Hot-driven rivets: technology, design and experiments [Ph.D. thesis], Vrije Universiteit Brussel; 2014.
- [5] Souto Carlos DS, Gomes Vítor MG, Da Silva Lucas FRC, Figueiredo Miguel V, Correia José AFO, Lesiuk Grzegorz, Fernandes António A, De Jesus Abílio MP. Global-local fatigue approaches for snug-tight and preloaded hot-dip galvanized steel bolted joints. Int J Fatigue 2021;153:106486.
- [6] Zampieri P, Curtarello A, Maiorana E, Pellegrino C. A review of the fatigue strength of shear bolted connections. Int J Steel Struct 2019;19:1084–98.
- [7] Maljaars Johan, Euler Mathias. Fatigue S-N curves of bolts and bolted connections for application in civil engineering structures. Int J Fatigue 2021;151:106355.
- [8] Maljaars Johan, Hengeveld Sjoerd, Rodenburg Jorrit. Fatigue driving force of riveted shear joints in bridges-replacing the net section stress. Int J Fatigue 2024;187:108466.
- [9] Fisher John W, Yen Ben T, Wang Dayi. Fatigue strength of riveted bridge members. J Struct Eng 1990;116:2968–81.
- [10] DiBattista Jeffrey D, Adamson Daniel EJ, Kulak Geoffrey L. Fatigue strength of riveted connections. J Struct Eng 1998;124:792–7.
- [11] Taras Andreas, Greiner Richard. Development and application of a fatigue class catalogue for riveted bridge components. Struct Eng Int 2010;20:91–103.
- [12] Pedrosa Bruno, Correia José AFO, Rebelo Carlos AS, Veljkovic Milan. Reliability of fatigue strength curves for riveted connections using normal and Weibull distribution functions. ASCE-ASME J Risk Uncertain Eng Syst Part A: Civ Eng 2020;6:04020034.
- [13] Graf O. Versuche mit Nietverbindungen Berichte des Deutschen Ausschusses für Stahlbau Heft 12. Springer-Verlag; 1941.
- [14] Parola JF, Chesson E, Munse WH. Effect of bearing pressure on fatigue strength of riveted connections. University of Illinois; 1965.
- [15] Baron F, Larson EW. Comparison of bolted and riveted joints. Trans. Am. Soc. Civil Eng. 1955;120:1322–34.
- [16] Wilson WM, Thomas FP. Fatigue tests of riveted joints. Tech. Rep., University of Illinois: 1938.
- [17] Pipinato Alessio, Molinari Marco, Pellegrino Carlo, Bursi Oreste S, Modena Claudio. Fatigue tests on riveted steel elements taken from a railway bridge. Struct Infrastruct Eng 2011;7:907–20.
- [18] EN1993-1-9+C2. Eurocode 3: Design of steel structures Part 1-9: Fatigue. CEN; 2012.
- [19] BS7608. Guide to fatigue design and assessment of steel products. BSI; 2014.
- [20] DNV RP C203. Recommended practice Fatigue design of offshore steel structures. DNV; 2024.
- [21] Munse WH. Riveted and bolted structural joints. Tech. Rep., University of Illinois; 1970.
- [22] Imam Boulent M, Righiniotis Timothy D, Chryssanthopoulos Marios K. Numerical modelling of riveted railway bridge connections for fatigue evaluation. Eng Struct 2007;29:3071–81.

- [23] Imam BM, Chryssanthopoulos MK, Frangopol DM. System effects on the fatigue reliability of deteriorating riveted railway bridges. In: Safety, reliability and risk of structures, infrastructures and engineering systems: proc. 10th int. conf. structural safety and reliability. 2009, p. 1–8.
- [24] De Jesus AMP, Silva AL, Correia JAFO. Fatigue of riveted and bolted joints made of puddle iron — a numerical approach. J Construct Steel Res 2014;102:164–77.
- [25] Sanches Rui F, De Jesus Abílio MP, Correia José AFO, Da Silva ALL, Fernandes AA. A probabilistic fatigue approach for riveted joints using Monte Carlo simulation. J Constr Steel Res 2015;110:149–62.
- [26] Horas CS, De Jesus AMP, Rui Calçada. Efficient computational approach for fatigue assessment of riveted connections. J Constr Steel Res 2019;153:1–18.
- [27] Leonetti Davide, Maljaars Johan, Snijder HH. Fatigue life prediction of hotriveted shear connections using system reliability. Eng Struct 2019;186:471–83.
- [28] Liu Z, Correia JAFO, Carvalho H, Mourão A, De Jesus A, Calçada R, Berto Filippo. Global-local fatigue assessment of an ancient riveted metallic bridge based on submodelling of the critical detail. Fatigue Fract Eng Mater Struct 2019;42:546–60.
- [29] Correia José AFO, da Silva António LL, Xin Haohui, Lesiuk Grzegorz, Zhu Shun-Peng, de Jesus Abílio MP, Fernandes António A. Fatigue performance prediction of S235 base steel plates in the riveted connections. Structures 2021;30:745–55.
- [30] Livieri Paolo. Numerical analysis of double riveted lap joints. Lubricants 2023;11:396.
- [31] Baron F, Larson EW, Kenworthy KJ. The effect of certain rivet patterns on the fatigue and static strengths of joints. Tech. rep., Northwestern University; 1955.
- [32] 2230:2015 VDI. Systematic calculation of high duty bolted joints. VDI; 2015.
- [33] Pascual FG, Meeker WQ. Analysis of fatigue data with runouts based on a model with nonconstant standard deviation and a fatigue limit parameter. Tech. rep., Department of Statistics, Iowa State University; 1996.
- [34] Pascual FG, Meeker WQ. Estimating fatigue curves with the random fatigue limit model. Technometrics 1999;41:277–89.
- [35] Castillo Enrique, Fernández-Canteli Alfonso. A unified statistical methodology for modeling fatigue damage. Springer Science & Business Media; 2009.
- [36] Hobbacher AF, et al. Recommendations for fatigue design of welded joints and components, vol. 47, Springer; 2016.
- [37] Bartsch Helen, Drebenstedt Karl, Seyfried Benjamin, Feldmann Markus, Kuhlmann Ulrike, Ummenhofer Thomas. Analysis of fatigue test data to reassess EN 1993-1-9 detail categories. Steel Constr 2020;13:280–93.
- [38] Schneider CRA, Maddox SJ. Best practice guide on statistical analysis of fatigue data. TWI doc. 13604.01/02/1157.02. Tech. Rep., The Welding Institute; 2003.
- [39] Drebenstedt K, Euler M. Statistical analysis of fatigue test data according to eurocode 3. In: Proc. maintenance, safety, risk, management and life-cycle performance of bridges. 2018, p. 2244–51.
- [40] JCSS. Probabilistic model code. JCSS; 2002, URL https://www.jcss-lc.org/jcss-probabilistic-model-code/.
- [41] Wells PL. Fatigue tests on steel bolts Offshore technology report OTO 97067.
  Tech. rep., Health and Safety Executive; 1998.
- [42] Hashimura Shinji, Socie Darrell F. A study of loosening and fatigue failure of bolted joints under transverse vibration. Trans Jpn Soc Mech Eng C 2006;72:1297–304.
- [43] Riveros GA, Mahmoud HN. Multiaxial fatigue strength of structural bolts under combined cyclic axial and shear demands. Tech. rep., U.S. Army Engineer Research and Development Center; 2019.
- [44] Wichtowski B. Untersuchungen zur Ermüdungsfestigkeit von Paßschrauben beim Abscheren. Stahlbau 2007;76:235–40.
- [45] Zhang Ming, Jiang Yanyao, Lee Chu-Hwa. An experimental investigation of the effects of clamped length and loading direction on self-loosening of bolted joints. ASME Press Vessel Pip Conf 2006;128:388–93.
- [46] Friede R, Lange J. Self loosening of prestressed bolts. In: Nordic steel construction conference NSCC2009, Malmö. Citeseer; 2009, p. 272–9.
- [47] Liu Jianhua, Mi Xue, Hu Huamin, Long Laohu, Cai Zhenbing, Peng Jinfang, Zhu Minhao. Loosening behaviour of threaded fasteners under cyclic shear displacement. Wear 2020;460:203453.
- [48] Brühwiler E, Hirt MA. Das Ermüdungsverhalten genieteter Brückenbauteile. Stahlbau 1987:56:1–8.
- [49] Brühwiler Eugen, Smith Ian FC, Hirt Manfred A. Fatigue and fracture of riveted bridge members. J Struct Eng 1990;116:198–214.
- [50] Pipinato A, Pellegrino C, Bursi OS, Modena C. High-cycle fatigue behavior of riveted connections for railway metal bridges. J Constr Steel Res 2009:65:2167–75.
- [51] Graf O. Dauerversuche mit Nietverbindungen in St37 zur Erkennung des Einflusses von  $\sigma$ :  $\tau$ . Der Bauingenieur 1932;29/30:389–93.
- [52] Wilson WM. Flexural fatigue strength of steel beams. Tech. Rep., Bulletin 45. University of Illinois; 1948.
- [53] Leonetti D, Maljaars J, Pasquarelli G, Brando G. Rivet clamping force of as-built hot-riveted connections in steel bridges. J Constr Steel Res 2020;167:105955.
- [54] Kulak GL, Fisher JW, Struik JHA. Guide to design criteria for bolted and riveted joints. 2nd ed.. American Institute of Steel Construction (AISC); 2001.
- [55] FKM:2012. Rechnerischer Festigkeitsnachweis für Maschinenbauteile. VDMA Verlag GmbH; 2012.

- [56] White DJ. Fatigue strength of small pinned connections made from alloy steel FV 520B. Proc Inst Mech Eng 1967;182:615–30.
- [57] Meggiolaro Marco Antonio, Pinho de Castro Jaime Tupiassú, Wu Hao. Static axial tension or compression stress effects on shear cracks initiating under cyclic torsion loads in multiaxial fatigue tests. Int J Fatigue 2024;179:108021.
- [58] Heirani Hasan, Farhangdoost Khalil. Effect of compressive Mode I on the mixed Mode I/II fatigue crack growth rate of 42CrMo4. J Mater Eng Perform 2018;27:138–46.
- [59] Davoli P, Bernasconi AA, Filippini M, Foletti S. Independence of the torsional fatigue limit upon a mean shear stress. Int J Fatigue 2003;25:471–80.
- [60] Bartsch Helen, Feldmann Markus. Revision of fatigue detail categories of plain members and mechanically fastened joints according to EC3-1-9. J Constr Steel Res 2021;179:106549.
- [61] Farris TN, Murthy H, Matlik JF. 4.11 fretting fatigue. In: Comprehensive structural integrity. Oxford: Pergamon; 2003, p. 281–326. http://dx.doi.org/10.1016/B0-08-043749-4/04080-5, URL https://www.sciencedirect.com/science/article/pii/B0080437494040805.

- [62] Groper M. Microslip and macroslip in bolted joints. Exp Mech 1985;25:171-4.
- [63] Ibrahim RA, Pettit CL. Uncertainties and dynamic problems of bolted joints and other fasteners. J Sound Vib 2005;279:857–936.
- [64] Ince A. A mean stress correction model for tensile and compressive mean stress fatigue loadings. Fatigue Fract Eng Mater Struct 2017;40:939–48.
- [65] Graf O. Versuche im Stahlbau Dauerversuche mit Nietverbindungen. Berichte Deutsche Ausschusses für Stahlbau 1935;5:1–61.
- [66] Chen Yu, Yamaguchi Takashi, Yamauchi Motoshi, Ueno Keita. Slip coefficient of 90-year-old riveted joint surface with red lead paint for corrosion. In: Proc. IABSE congress Ghent. 2021, p. 598–604.
- [67] Taras Andreas, Greiner Richard. Statische Festigkeit und Ermüdungsfestigkeit genieteter Bauteile - Auswertung der Versuchsdaten und Bemessungsvorschläge. Tech. rep., Graz University of Technology; 2007.